Journal of Computational Physics 230 (2011) 2189–2206

Contents lists available at ScienceDirect

Journal of Computational Physics

journal homepage: www.elsevier.com/locate/jcp

Efficient Arnoldi-type algorithms for rational eigenvalue problems arising in fluid–solid systems

So-Hsiang Chou [a,*], Tsung-Ming Huang [b], Wei-Qiang Huang [c], Wen-Wei Lin [d]

[a] Department of Mathematics and Statistics, Bowling Green State University, Bowling Green, OH 43403-0221, USA
[b] Department of Mathematics, National Taiwan Normal University, Taipei 116, Taiwan
[c] Department of Applied Mathematics, National Chiao Tung University, Hsinchu 300, Taiwan
[d] Department of Mathematics, National Taiwan University, Taipei 106, Taiwan

ARTICLE INFO

Article history:
Received 31 August 2010
Received in revised form 14 December 2010
Accepted 14 December 2010
Available online 21 December 2010

Keywords:
Fluid–structure interaction
Finite elements
Rational eigenvalue problem
Trimmed linearization
Arnoldi algorithm

ABSTRACT

We develop and analyze efficient methods for computing damped vibration modes of an acoustic fluid confined in a cavity with absorbing walls capable of dissipating acoustic energy. The discretization in terms of pressure nodal finite elements gives rise to a rational eigenvalue problem. Numerical evidence shows that there are no spurious eigenmodes for such discretization and also confirms that the discretization based on nodal pressures is much more efficient than that based on Raviart–Thomas finite elements for the displacement field. The trimmed linearization method is used to linearize the associated rational eigenvalue problem into a generalized eigenvalue problem (GEP) of the form $\mathcal{A}x = \lambda\mathcal{B}x$. For solving the GEP we apply Arnoldi algorithm to two different types of single matrices $\mathcal{B}^{-1}\mathcal{A}$ and $\mathcal{A}\mathcal{B}^{-1}$. Numerical accuracy shows that the application of Arnoldi on $\mathcal{A}\mathcal{B}^{-1}$ is better than that on $\mathcal{B}^{-1}\mathcal{A}$.

© 2010 Elsevier Inc. All rights reserved.

1. Introduction

Efficient and correct computation of the damped vibration modes generated by an inviscid, compressible, barotropic fluid in a cavity with absorbing walls is an important issue when for example one is interested in decreasing the level of noise in aircraft or cars. In general, one needs first a mathematical model consisted of partial differential equations with proper boundary and initial conditions. After this first phase of mathematical formulation, the next phase is to find efficient methods to compute the modes. This phase involves correct discretization of the mathematical formulation and computation of large scale nonlinear eigenvalue problems, be it quadratic, cubic, or even rational. Choosing correct discretization schemes to avoid spurious modes and finding efficient methods to locate eigenvalues that lie in the interior of the spectrum are among important issues to deal with. In the mathematical formulation phase, we have interaction between the fluid and structure (cavity walls), and the displacement variable natural for the solid could be chosen for the fluid as well so that compatibility and equilibrium (cf. (2.3) and (2.7) below) through the fluid–solid interface can be satisfied automatically. A drawback lurking behind the displacement formulation is the possible presence of nonphysical zero-frequency spurious circulation modes, if one is not careful in choosing the discretization scheme associated with the underlying partial differential system. For example discretization by standard finite elements or finite differences often exhibit such a phenomenon. Approaches circumventing this drawback can be found in [2,8,11,12,29], among others.

* Corresponding author. Tel.: +1 419 372 8225; fax: +1 419 372 6092.
E-mail addresses: chou@bgnet.bgsu.edu (S.-H. Chou), min@math.ntnu.edu.tw (T.-M. Huang), wqhuang@g2.nctu.edu.tw (W.-Q. Huang), wwlin@math.ntu.edu.tw (W.-W. Lin).

0021-9991/$ - see front matter © 2010 Elsevier Inc. All rights reserved.
doi:10.1016/j.jcp.2010.12.022

One of the discretizations we will be using in this paper is the edge-based or Raviart–Thomas finite elements for the displacement field, following [3,5]. The main concerns in [3,19] are pure mathematical issues of proving that their numerical approximation is free of spurious modes and has second order convergence rate. Efficient computation of the modes is not a concern, as they solved the associated quadratic eigenvalue problem by the standard eigensolver *eigs* from Matlab that employs Arnoldi iterations.

In this paper our primary concern is to develop and study efficient eigensolvers for the spectral approximation of the damped vibration modes. Two approximations are investigated, one constructed from the edge-based displacement space (cf. Eq. (2.11) below), which results in quadratic eigenvalue problems (QEPs) and one from the node-based pressure space (cf. Eq. (2.12)), which results in rational eigenvalues problems (REPs). Our first approximation is identical to that in [3,5], but we further develop efficient methods for solving the associated QEP. However, we show in Section 2 that this problem has a large zero-frequency or null space and this fact may influence the efficiency of Arnoldi-type algorithms. Motivated by this, we extensively explore the second approximation of using the pressure space, which has a much smaller eigenvalue system to solve and which has a one dimensional null space. Instead of a QEP, the associated eigenvalue problem is a rational one having the form $R(\lambda)\mathbf{p} = 0$, where $R(\lambda) := \lambda^2 M + \frac{\lambda^2}{\alpha+\beta\lambda} A + K$ is the rational λ-matrix with coefficient matrices M, A and K. While there is an extensive literature on QEPs problems [26], REPs are much less studied [25,27,28]. Although on the surface the rational $R(\lambda)\mathbf{p} = 0$ could be turned into a cubic one by multiplying out the denominator, we will preserve its rational structure and design efficient methods to numerically solve it in Section 3.

The organization of this paper is as follows. We describe the underlying model fluid–solid problem of this paper in Section 2, where the edge-based displacement approximation and the node-based pressure approximation are derived. We pay particular attention to identifying the dimension of the associated null space, which may influence performance of the numerical method introduced later. In Section 3, we use the general strategy of turning a nonlinear eigenvalue problem into a standard one by some sort of linearization techniques. We then apply the Arnoldi type algorithms to solve it. For the two nonlinear eigenvalue problems, the QEP is as usual turned into a generalized eigenvalue problem (GEP), from which two types of standard eigenvalue problems (SEP) (3.7.1) and (3.7.2) are derived. The REP is trimmed-linearized into two types of three by three block SEPs (3.19.1) and (3.19.2). The important issue of residual error bound analysis is addressed here. We then apply Arnoldi method with Schur-restarting described in Section 4 to the resulting SEPs. The important issues of stopping criteria and computational costs for applying Arnoldi method to the QEP and REP are also derived in this section. In Section 5, we present numerical results and evaluate the merits of the schemes involved where we also demonstrate the role of normwise scaling in preprocessing the eigenvalue problems. Conclusions are included in Section 6.

2. Model problem

Let us consider a simple model of a rigid container filled with an inviscid compressible barotropic fluid and its acoustic energy is absorbed through a thin layer of a viscoelastic material applied to some or all of its walls. For simplicity we assume the fluid domain $\Omega \subset \mathbf{R}^n$ ($n = 2$ or 3) to be polyhedral, and the boundary $\partial\Omega = \Gamma_A \cup \Gamma_R$, where the absorbing boundary Γ_A is the union of all the different faces of Ω and is covered by damping material. The rigid boundary Γ_R is the remaining part of Γ. An example of the setup is in Fig. 1(i) on Section 5, where the top boundary is absorbing and the remaining boundary is rigid.

The dynamic variables of our model problem are the fluid pressure P and the displacement field $\mathbf{U}$, which satisfy ([6,15])

$$\rho \frac{\partial^2 \mathbf{U}}{\partial t^2} + \nabla P = \mathbf{0} \quad \text{in } \Omega, \tag{2.1}$$

$$P = -\rho c^2 \operatorname{div} \mathbf{U} \quad \text{in } \Omega, \tag{2.2}$$

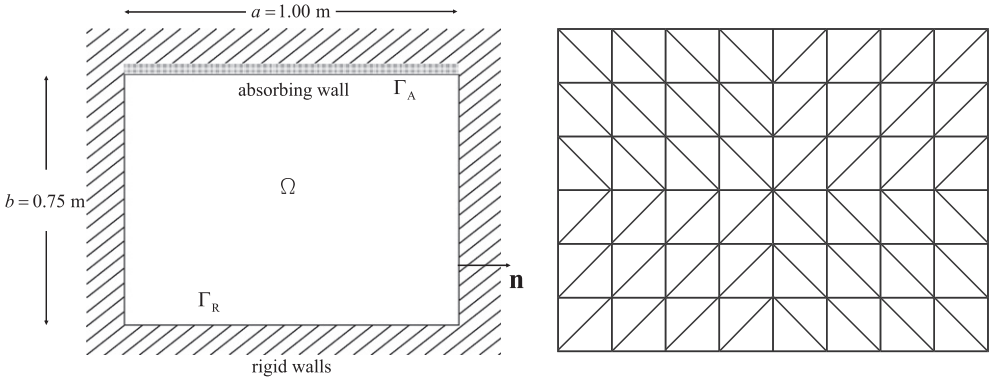

(i) Fluid in a cavity with one absorbing wall. (ii) Initial mesh.

Fig. 1. Fluid in a cavity with one absorbing wall and initial mesh.

$$P = \left(\alpha \mathbf{U}\cdot\mathbf{n} + \beta \frac{\partial \mathbf{U}}{\partial t}\cdot\mathbf{n}\right) \quad \text{on } \Gamma_A, \tag{2.3}$$

$$\mathbf{U}\cdot\mathbf{n} = 0 \quad \text{on } \Gamma_R. \tag{2.4}$$

Here ρ is the fluid density, c, the acoustic speed, and $\mathbf{n}$, the unit outer normal vector along $\partial\Omega$. At the absorbing boundary (2.3) indicates that the pressure is balanced by the effects of the viscous damping (the β term) and the elastic behavior (the α term). We assume the coefficients α and β are given positive constants.

To look for the damped vibration modes we assume (2.1)–(2.4) has complex solution of the form $\mathbf{U}(\mathbf{x},t) = e^{\lambda t}\mathbf{u}(\mathbf{x})$ and $P(\mathbf{x},t) = e^{\lambda t}p(\mathbf{x})$. This leads to a problem of finding $\lambda \in \mathbb{C}, \mathbf{u} : \Omega \to \mathbb{C}^n$ and $p : \Omega \to \mathbb{C}, (\mathbf{u},p) \neq (\mathbf{0},0)$ such that

$$\rho\lambda^2\mathbf{u} + \nabla p = \mathbf{0} \quad \text{in } \Omega, \tag{2.5}$$

$$p = -\rho c^2 \operatorname{div}\mathbf{u} \quad \text{in } \Omega, \tag{2.6}$$

$$p = (\alpha + \lambda\beta)\mathbf{u}\cdot\mathbf{n} \quad \text{on } \Gamma_A, \tag{2.7}$$

$$\mathbf{u}\cdot\mathbf{n} = 0 \quad \text{on } \Gamma_R. \tag{2.8}$$

The boundary condition (2.7) makes this eigenvalue problem nonlinear. For each damped vibration mode, $\omega := \mathrm{Im}\lambda$ is the vibration angular frequency and $\mathrm{Re}\lambda$ the decay rate. In practice, we select a range of ω values and are interested in the least decaying modes in this range. We next describe the natural variational formulation of the above problem on which the numerical approximation will be based.

Let

$$\mathcal{V} := \{\mathbf{v} \in H(\operatorname{div},\Omega) : \mathbf{v}\cdot\mathbf{n} \in L^2(\partial\Omega) \quad \text{and} \quad \mathbf{v}\cdot\mathbf{n} = 0 \text{ on } \Gamma_R\}.$$

Here we employ standard Sobolev spaces notation. For example, $H(\operatorname{div},\Omega)$ stands for the space of all L^2 vector functions $\mathbf{v}$ on Ω with L^2 integrable divergence.

Testing (2.5) by $\bar{\mathbf{v}} \in \mathcal{V}$ and integrating by parts, we obtain a variational formulation of problem (2.5)–(2.8) involving only the displacement variable: Find $\lambda \in \mathbb{C}$ and $\mathbf{u} \in \mathcal{V}, \mathbf{u} \neq \mathbf{0}$, such that

$$\int_\Omega \rho c^2 \operatorname{div}\mathbf{u} \operatorname{div}\bar{\mathbf{v}} + \int_{\Gamma_A} \alpha \mathbf{u}\cdot\mathbf{n}\bar{\mathbf{v}}\cdot\mathbf{n} + \lambda\int_{\Gamma_A}\beta\mathbf{u}\cdot\mathbf{n}\bar{\mathbf{v}}\cdot\mathbf{n} + \lambda^2\int_\Omega \rho\mathbf{u}\cdot\bar{\mathbf{v}} = 0 \quad \forall\, \mathbf{v} \in \mathcal{V}. \tag{2.9}$$

(We use the symbol $\forall$ to mean 'for all' throughout the paper.) This is a quadratic eigenvalue problem. Note that $\lambda = 0$ is an eigenvalue and the dimension of its eigenspace

$$\mathcal{K} := \{\mathbf{u} \in \mathcal{V} : \ \operatorname{div}\mathbf{u} = 0 \text{ in } \Omega \quad \text{and} \quad \mathbf{u}\cdot\mathbf{n} = \mathbf{0} \text{ on } \partial\Omega\}$$

is infinity. All nonzero eigenvalues have finite multiplicity (the dimension of the eigenspace is finite) [4]. It is shown in [4] that all the other solutions of (2.9), the decay rate is strictly negative. That is, if an eigenpair $0 \neq \lambda \in \mathbf{C}$ and $\mathbf{0} \neq \mathbf{u} \in \mathcal{V}$ is a solution of problem (2.9) then $\mathrm{Re}\lambda < 0$.

Alternatively we can derive a variational formulation in terms of the pressure: Find $\lambda \in \mathbb{C}$ and $p \in H^1(\Omega)$ such that

$$\int_\Omega \nabla p\cdot\nabla\bar{q} + \frac{\lambda^2}{\alpha+\lambda\beta}\int_{\Gamma_A}\rho p\bar{q} + \frac{\lambda^2}{c^2}\int_\Omega p\bar{q} = 0 \quad \forall\, q \in H^1(\Omega). \tag{2.10}$$

However, in this case the eigenvalue problem is rational, which is rarely studied compared with linear and quadratic eigenvalue problems. Note that in contrast to the displacement formulation, the eigenspace corresponding to $\lambda = 0$ is now one dimensional. Thus this formulation has a much smaller null space or kernel, which may be more stable and efficient when used in conjunction with projection-like spectral approximation methods.

2.1. Spectral approximation

We now turn to the finite element methods for approximating the solutions of the quadratic eigenvalue problem (2.9) and the rational eigenvalue problem (2.10). Spurious modes are usually present when standard finite elements are used in a displacement formulation. However Bermúdez et al. [4] successfully demonstrated that the spurious modes can be avoided by using the lowest order Raviart–Thomas elements in $\mathbb{R}^n, n = 2,3$ (see, for instance, [7,18]). For simplicity we will consider only the two dimensional case. Let $\{\mathcal{T}_h\}$ be a regular family of triangulations of Ω indexed by h, the maximum diameter of the elements. Let

$$\mathcal{V}_h := \{\mathbf{v}_h \in H(\operatorname{div},\Omega) : \mathbf{v}_h|_T \in \mathcal{P}_0^n \oplus \mathcal{P}_0\mathbf{x} \quad \forall\, T \in \mathcal{T}_h \quad \text{and} \quad \mathbf{v}_h\cdot\mathbf{n} = 0 \text{ on } \Gamma_R\} \subset \mathcal{V}$$

where $n = 2$ and $\mathcal{P}_k$ denotes the set of polynomials of degree at most k. Thus locally $\mathbf{v}_h$ takes the form $(a+sx, b+sy)^\top$ ($\top$ denotes transpose and $\mathbf{x} = (x,y)^\top$). The discrete problem associated with (2.9) is: Find $\lambda \in \mathbb{C}$ and $\mathbf{u}_h \in \mathcal{V}_h, \mathbf{u}_h \neq \mathbf{0}$, such that

$$\int_\Omega \rho c^2 \operatorname{div}\mathbf{u}_h \operatorname{div}\bar{\mathbf{v}}_h + \int_{\Gamma_A}\alpha\mathbf{u}_h\cdot\mathbf{n}\bar{\mathbf{v}}_h\cdot\mathbf{n} + \lambda\int_{\Gamma_A}\beta\mathbf{u}_h\cdot\mathbf{n}\bar{\mathbf{v}}_h\cdot\mathbf{n} + \lambda^2\int_\Omega\rho\mathbf{u}_h\cdot\bar{\mathbf{v}}_h = 0, \quad \forall\, \mathbf{v}_h \in \mathcal{V}_h. \tag{2.11}$$

Theorem 1. *The dimension of the zero eigenspace $\mathcal{E}_0$ associated with (2.11) equals the number of interior nodes in the triangulation.*

Proof. Setting $\mathbf{v}_h = \mathbf{u}_h$ and $\lambda = 0$ in (2.11), we see that

$$\operatorname{div}\mathbf{u}_h = 0 \text{ on } \Omega \quad \text{and} \quad \mathbf{u}_h \cdot \mathbf{n} = 0 \text{ on } \partial\Omega.$$

Since $\mathbf{u}_h = (a + sx, b + sy)^\top$ on $T \in \mathcal{T}_h$, the divergence free condition implies that $\mathbf{u}_h$ is a constant vector $(a,b)^\top$ on T. By direct computation, we see that there exists a linear polynomial ψ_T such that

$$\frac{\partial \psi_T}{\partial x} = -b \quad \text{and} \quad \frac{\partial \psi_T}{\partial y} = a.$$

Let $\mathbf{n} = (n_1, n_2)^\top$ be a unit normal to an edge e of T, so $\mathbf{t} = (-n_2, n_1)^\top$ is a unit tangent vector to e. We see that

$$\mathbf{u}_h \cdot \mathbf{n} = \nabla \psi_T \cdot \mathbf{t} = \frac{\partial \psi_T}{\partial \mathbf{t}}.$$

So if an edge e is common to T_1 and T_2 then in general ψ_{T_1} and ψ_{T_2} differ by a constant only by the continuity of $\mathbf{u}_h \cdot \mathbf{n}$ across e. At an interior node N_j, we can assign a common value for all ψ_T at that node. Here T are all triangles sharing N_j as the common node. We then spread this defining process outward to all Ω using the induced values on other nodes. Consequently, Ψ is continuous piecewise linear over Ω. Let $\nabla^\perp := (-\frac{\partial}{\partial y}, \frac{\partial}{\partial x})^\top$ and define

$$\nabla^\perp S_h := \{\nabla^\perp \Psi_h : \Psi_h \text{ is continuous piecewise linear and vanishes on the boundary}\}.$$

Thus we have just shown the zero eigenspace $\mathcal{E}_0$ is contained $\nabla^\perp S_h$ and the opposite inclusion is also easily checked. Hence

$$\mathcal{E}_0 = \nabla^\perp S_h.$$

We now find the dimension of $\nabla^\perp S_h$. Let N be the number of interior nodes and let $\Psi_j, j = 1, \ldots, N$, be the nodal basis functions such that $\Psi_j(N_k) = \delta_{kj}$. The linear independence of Ψ_j's is preserved by the perp-gradient operation. In fact, suppose $\sum_{j=1}^N c_j \nabla^\perp \Psi_j = 0$. Then this implies $\sum_{j=1}^N c_j \Psi_j = c$ for some constant c. Hence $c_j = c$ by the condition $\Psi_j(N_k) = \delta_{kj}$. Consequently, $c(\sum_j \Psi_j - 1) = 0$. But we know $\sum_{j=1}^N \Psi_j \neq 1$ due to the vanishing boundary condition. Thus $c_j = c = 0$ and we conclude that the dimension of the zero eigenspace $\dim\mathcal{E}_0 = \dim\nabla^\perp S_h$ equals the number of interior nodes in the mesh. □

Define the conforming P_1 finite element space

$$H_h := \{p_h \in H^1(\Omega) : p_h|_T \in \mathcal{P}_1 \quad \forall\, T \in \mathcal{T}_h\}.$$

This is the subspace of $H^1(\Omega)$ consisted of continuous piecewise linears. The alternative discrete problem in terms of the approximate pressure field is: Find $\lambda \in \mathbb{C}$ and $p_h \in H_h$ such that

$$\int_\Omega \nabla p_h \cdot \nabla \bar{q}_h + \frac{\lambda^2}{\alpha + \lambda\beta} \int_{\Gamma_A} \rho p_h \bar{q}_h + \frac{\lambda^2}{c^2} \int_\Omega p_h \bar{q}_h = 0 \quad \forall\, q_h \in H_h. \tag{2.12}$$

Letting $q_h = p_h$ and $\lambda = 0$ in (2.12) we can easily see that the dimension of the zero eigenspace in this case is one, which is the same as the original problem (2.10).

Again we see that the pressure formulation has a much smaller null space than the displacement formulation. Also the number of unknowns is much smaller. Thus the pressure formulation turns out to be a very good alternative, once in addition we show in the remaining sections that its associated eigenvalue problem can be efficiently solved. A minor remark is in order here.

Remark 2.1. Suppose an eigenpair $(\lambda, p_h), \lambda \neq 0$ has been computed, what if, in addition, one wants to know a corresponding displacement approximation $\mathbf{u}_h$? One must not find $\mathbf{u}_h$ by solving an additional system linear equations again so as to maintain the advantage of the pressure formulation. It should be given by a simple formula. A naive way is to use the relation (2.5) to evaluate a $\mathbf{u}_h$, but this would be ill conceived since the computed displacement would be piecewise constant. Consequently, $\nabla \cdot \mathbf{u}_h = 0$, which certainly does not approximate (2.6). Fortunately, a general principle for such a problem (recovery of $\mathbf{u}_h$ from the pressure approximation p_h) has been provided in [9] where one can obtain an accurate $\mathbf{u}_h$ in the Raviart–Thomas space by a simple evaluation formula which is a modification of the above naive formula.

3. Linearization of nonlinear eigenvalue problems

In this section we start to address the computational issues related to the displacement approximation (2.11) and the pressure approximation (2.12).

3.1. Linearization of quadratic eigenvalue problem

Suppose the total number of interior and absorbing edges is n_1. Let $\{\phi_j\}_{j=1}^{n_1}$ denote the cardinal basis of $\mathcal{V}_h$, so that on the edge e_j, ϕ_j has the unit normal flux and zero normal flux on the remaining $n_1 - 1$ edges. That is, $\int_{e_i} \phi_j \cdot \mathbf{n}_i d\sigma = \delta_{ij}$. For $\mathbf{u}_h \in \mathcal{V}_h$, we write $\mathbf{u}_h = \sum_{j=1}^{n_1} u_j \phi_j$ and denote $\mathbf{u} = [u_1^\top, \cdots, u_{n_1}^\top]^\top$. Note that the unknown vector $\mathbf{u}$ contains normal fluxes in its components. Then, the discrete problem (2.11) can be expressed as the following QEP:

$$Q(\lambda)\mathbf{u} \equiv \lambda^2 M_u \mathbf{u} + (\alpha + \lambda\beta) A_u \mathbf{u} + K_u \mathbf{u} = 0, \tag{3.1}$$

where $M_u \equiv [M_{ij}^u]$ and $K_u \equiv [K_{ij}^u]$ are mass and stiffness matrices, respectively, and $A_u \equiv [A_{ij}^u]$ is used to describe the effect of the absorbing wall. Here

$$M_{ij}^u = \int_\Omega \rho \phi_i \cdot \bar{\phi}_j, \quad K_{ij}^u = \int_\Omega \rho c^2 \ \mathrm{div}\ \phi_i \ \mathrm{div}\ \bar{\phi}_j, \quad A_{ij}^u = \int_{\Gamma_A} \phi_i \cdot \mathbf{n} \bar{\phi}_j \cdot \mathbf{n}, \tag{3.2}$$

for $i, j = 1, \ldots, n_1$. For this problem, we are only interested in eigenvalues that are located in the interior of the spectrum. Suppose that the eigenvalues near σ are of interest. Accordingly, the QEP (3.1) is shifted into

$$\left(\mu^2 \widetilde{M}_u + \mu \widetilde{D}_u + \widetilde{K}_u\right)\mathbf{u} = 0 \tag{3.3}$$

with $\mu = \lambda - \sigma$ and

$$\widetilde{M}_u = M_u, \widetilde{D}_u = 2\sigma M_u + \beta A_u, \quad \widetilde{K}_u = \sigma^2 M_u + (\alpha + \sigma\beta) A_u + K_u. \tag{3.4}$$

On the one hand, one can numerically solve (3.3) without transforming it further. Among such direct methods we mention the SOAR (second-order Arnoldi) algorithm [1] and the Jacobi–Davidson algorithm applied to polynomial eigenvalue problems [21]. On the other hand, it is more common to transform or linearize (3.3) into a SEP [26]. In this paper, we let

$$\mathcal{A}_u = \begin{bmatrix} 0 & -\widetilde{M}_u \\ I & -\widetilde{D}_u \end{bmatrix}, \quad \mathcal{B}_u = \begin{bmatrix} I & 0 \\ 0 & \widetilde{K}_u \end{bmatrix} \tag{3.5}$$

and linearize (3.3) into the GEP

$$\mathcal{A}_u \mathbf{x} = \frac{1}{\mu} \mathcal{B}_u \mathbf{x} \quad \text{with } x \equiv \begin{bmatrix} -\mu \widetilde{M}_u \mathbf{u} \\ \mathbf{u} \end{bmatrix} \equiv \begin{bmatrix} \mathbf{v} \\ \mathbf{u} \end{bmatrix}. \tag{3.6}$$

The matrix $\widetilde{K}_u$ in (3.5) is nonsingular because the shift value σ is not an eigenvalue of (3.1). Furthermore, the GEP (3.6) can then be transformed into two types of SEPs of the forms $\mathcal{B}_u^{-1}\mathcal{A}_u\mathbf{x} = \mu^{-1}\mathbf{x}$ and $\mathcal{A}_u\mathcal{B}_u^{-1}\mathbf{y} = \mu^{-1}\mathbf{y}$, respectively, where $\mathbf{y} = \mathcal{B}_u\mathbf{x}$. Therefore, from (3.5) and (3.6) we have

$$(\mathbf{Q} - \mathbf{SEP1}) \quad \mathcal{B}_u^{-1}\mathcal{A}_u \begin{bmatrix} \mathbf{v} \\ \mathbf{u} \end{bmatrix} = \begin{bmatrix} 0 & -\widetilde{M}_u \\ \widetilde{K}_u^{-1} & -\widetilde{K}_u^{-1}\widetilde{D}_u \end{bmatrix} \begin{bmatrix} \mathbf{v} \\ \mathbf{u} \end{bmatrix} = \frac{1}{\mu} \begin{bmatrix} \mathbf{v} \\ \mathbf{u} \end{bmatrix} \tag{3.7.1}$$

and

$$(\mathbf{Q} - \mathbf{SEP2}) \quad \mathcal{A}_u\mathcal{B}_u^{-1} \begin{bmatrix} \mathbf{v} \\ \mathbf{w} \end{bmatrix} = \begin{bmatrix} 0 & -\widetilde{M}_u\widetilde{K}_u^{-1} \\ I & -\widetilde{D}_u\widetilde{K}_u^{-1} \end{bmatrix} \begin{bmatrix} \mathbf{v} \\ \mathbf{w} \end{bmatrix} = \frac{1}{\mu} \begin{bmatrix} \mathbf{v} \\ \mathbf{w} \end{bmatrix}, \quad \mathbf{w} = \widetilde{K}_u \mathbf{u}. \tag{3.7.2}$$

Note that the SEPs of (3.7.1) and (3.7.2) derived by the QEP in (3.3), are called **Q-SEP1** and **Q-SEP2**, respectively. The standard Arnoldi method can then be applied to solve **Q-SEP**s, and the details will be given in Section 4.

3.2. Trimmed linearization method for rational eigenvalue problem

Let $\{\psi_j\}_{j=1}^{n_2}$ be a nodal basis of H_h. For $p_h \in H_h$, we write $p_h = \sum_{j=1}^{n_2} p_j \psi_j$ and denote $\mathbf{p} = [p_1, \cdots, p_{n_2}]^\top$. Then, the discrete problem (2.12) can be written as the following REP:

$$R(\lambda)\mathbf{p} \equiv \left(\frac{\lambda^2}{c^2} M_p + K_p + \frac{\lambda^2}{\lambda\beta + \alpha} A_p\right)\mathbf{p} = 0, \tag{3.8}$$

where $M_p \equiv [M_{ij}^p]$ and $K_p \equiv [K_{ij}^p]$ are mass and stiffness matrices, respectively, and $A_p \equiv [A_{ij}^p]$ describes the effect of the absorbing wall. Here,

$$M_{ij}^p = \int_\Omega \psi_i \bar{\psi}_j, \quad K_{ij}^p = \int_\Omega \nabla\psi_i \cdot \nabla\bar{\psi}_j, \quad A_{ij}^p = \int_{\Gamma_A} \rho \psi_i \bar{\psi}_j \tag{3.9}$$

for $i, j = 1, \ldots, n_2$.

To solve REP (3.8), one approach is to multiply equation (3.8) by the scalar $\lambda\beta+\alpha$ and expand it into a cubic polynomial eigenvalue problem, and then solve it by Jacobi–Davidson method [14]. An alternative approach is to treat (3.8) as nonlinear eigenvalue problem and solve it by a nonlinear eigensolver, such as Newton's method, nonlinear Arnoldi method, or nonlinear Jacobi–Davidson method [20,27,28]. Recently, a trimmed linearization is proposed in [25] which linearizes (3.8) into a GEP so that the standard Arnoldi method can be applied. We introduce the trimmed linearization below.

Given a shift value σ. With $\mu=\lambda-\sigma$, the rational λ-matrix $R(\lambda)$ in (3.8) can be rewritten as

$$\begin{aligned}
R(\lambda) &= \frac{(\lambda-\sigma+\sigma)^2}{c^2}M_p + K_p + \frac{(\lambda-\sigma+\sigma)^2}{(\lambda-\sigma+\sigma)\beta+\alpha}A_p \\
&= \frac{(\lambda-\sigma)^2+2(\lambda-\sigma)\sigma+\sigma^2}{c^2}M_p + K_p + \frac{(\lambda-\sigma)^2+2(\lambda-\sigma)\sigma+\sigma^2}{(\lambda-\sigma)\beta+\sigma\beta+\alpha}A_p \\
&= \mu^2\left(\frac{1}{c^2}M_p\right) + \mu\left(\frac{2\sigma}{c^2}M_p\right) + \left(\frac{\sigma^2}{c^2}M_p + K_p\right) + \frac{\mu^2+2\mu\sigma+\sigma^2}{\mu\beta+\sigma\beta+\alpha}A_p \\
&= \mu^2\left[\left(\frac{1}{c^2}M_p\right) + \frac{1}{\mu}\left(\frac{2\sigma}{c^2}M_p\right) + \frac{1}{\mu^2}\left(\frac{\sigma^2}{c^2}M_p + K_p\right) + \frac{1+2\sigma/\mu+\sigma^2/\mu^2}{\mu\beta+(\sigma\beta+\alpha)}A_p\right].
\end{aligned} \tag{3.10}$$

Setting $\nu=1/\mu$, the rational term in (3.10) can be simplified into the following form by applying the long division

$$\frac{\sigma^2\nu^2+2\sigma\nu+1}{\beta/\nu+(\sigma\beta+\alpha)} = \frac{\sigma^2}{\sigma\beta+\alpha}\nu^2 + \frac{\sigma^2\beta+2\sigma\alpha}{(\sigma\beta+\alpha)^2}\nu + \frac{\alpha^2}{(\sigma\beta+\alpha)^3} - \left(\frac{(\sigma\beta+\alpha)^3}{\alpha^2} + \frac{(\sigma\beta+\alpha)^4}{\alpha^2\beta}\nu\right)^{-1}.$$

This implies that

$$\begin{aligned}
R(\lambda) = \frac{1}{\nu^2}\Bigg[&\nu^2\left(\frac{\sigma^2}{c^2}M_p + K_p + \frac{\sigma^2}{\sigma\beta+\alpha}A_p\right) + \nu\left(\frac{2\sigma}{c^2}M_p + \frac{\sigma^2\beta+2\sigma\alpha}{(\sigma\beta+\alpha)^2}A_p\right) + \left(\frac{1}{c^2}M_p + \frac{\alpha^2}{(\sigma\beta+\alpha)^3}A_p\right) \\
&-\left(\frac{(\sigma\beta+\alpha)^3}{\alpha^2} + \frac{(\sigma\beta+\alpha)^4}{\alpha^2\beta}\nu\right)^{-1}A_p\Bigg] = \mu^2\widetilde{M}_p + \mu\widetilde{D}_p + \widetilde{K}_p - \mu^2(\vartheta-\varrho\mu^{-1})^{-1}L_pR_p^\top,
\end{aligned} \tag{3.11}$$

where

$$\widetilde{M}_p = \frac{1}{c^2}M_p + \frac{\alpha^2}{(\sigma\beta+\alpha)^3}A_p, \tag{3.12}$$

$$\widetilde{D}_p = \frac{2\sigma}{c^2}M_p + \frac{\sigma^2\beta+2\sigma\alpha}{(\sigma\beta+\alpha)^2}A_p, \tag{3.13}$$

$$\widetilde{K}_p = \frac{\sigma^2}{c^2}M_p + K_p + \frac{\sigma^2}{\sigma\beta+\alpha}A_p, \tag{3.14}$$

$$\vartheta = \frac{(\sigma\beta+\alpha)^3}{\alpha^2}, \quad \varrho = -\frac{(\sigma\beta+\alpha)^4}{\alpha^2\beta} \tag{3.15}$$

and $L_pR_p^\top = A_p$ is the full-rank decomposition of A_p with $L_p, R_p \in \mathbb{R}^{n_2\times m}$. Introducing an auxiliary vector

$$\mathbf{q} = (\vartheta-\varrho\mu^{-1})^{-1}R_p^\top\mathbf{p}, \tag{3.16}$$

the REP in (3.8) can be reformulated as

$$\left(\mu^2\widetilde{M}_p + \mu\widetilde{D}_p + \widetilde{K}_p\right)\mathbf{p} - \mu^2L_p\mathbf{q} = 0. \tag{3.17}$$

Using (3.16) and (3.17), we get the GEP

$$\mathcal{A}_p\mathbf{x} \equiv \begin{bmatrix} 0 & -\widetilde{M}_p & L_p \\ I_{n_2} & -\widetilde{D}_p & 0 \\ 0 & -R_p^\top & \vartheta I_m \end{bmatrix}\mathbf{x} = \frac{1}{\mu}\begin{bmatrix} I_{n_2} & 0 & 0 \\ 0 & \widetilde{K}_p & 0 \\ 0 & 0 & \varrho I_m \end{bmatrix}\mathbf{x} \equiv \frac{1}{\mu}\mathcal{B}_p\mathbf{x}, \tag{3.18}$$

where $\mathbf{x} = [((\mu^{-1}\widetilde{K}_p+\widetilde{D}_p)\mathbf{p})^\top, \mathbf{p}^\top, \mathbf{q}^\top]^\top$. As before, the matrix $\widetilde{K}_p$ in (3.14) is nonsingular because the shift value σ is not an eigenvalue of (3.8). As in (3.7.1) and (3.7.2), the GEP (3.18) can then be, respectively, transformed into the following two types of the SEPs of the forms $\mathcal{B}_p^{-1}\mathcal{A}_p\mathbf{x} = \mu^{-1}\mathbf{x}$ and $\mathcal{A}_p\mathcal{B}_p^{-1}\mathbf{y} = \mu^{-1}\mathbf{y}$ where $\mathbf{y} = \mathcal{B}_p\mathbf{x}$. Consequently, we have

$$(\mathbf{R}-\mathbf{SEP1})\quad \mathcal{B}_p^{-1}\mathcal{A}_p\mathbf{x}=\begin{bmatrix}0 & -\widetilde{M}_p & L_p\\ \widetilde{K}_p^{-1} & -\widetilde{K}_p^{-1}\widetilde{D}_p & 0\\ 0 & -\varrho^{-1}R_p^{\top} & \varrho^{-1}\vartheta I_m\end{bmatrix}\mathbf{x}=\frac{1}{\mu}\mathbf{x}, \tag{3.19.1}$$

and

$$(\mathbf{R}-\mathbf{SEP2})\quad \mathcal{A}_p\mathcal{B}_p^{-1}\mathbf{y}=\begin{bmatrix}0 & -\widetilde{M}_p\widetilde{K}_p^{-1} & \varrho^{-1}L_p\\ I_{n_2} & -\widetilde{D}_p\widetilde{K}_p^{-1} & 0\\ 0 & -R_p^{\top}\widetilde{K}_p^{-1} & \varrho^{-1}\vartheta I_m\end{bmatrix}\mathbf{y}=\frac{1}{\mu}\mathbf{y},\quad \mathbf{y}=\mathcal{B}_p\mathbf{x}. \tag{3.19.2}$$

Note that the SEPs of (3.19.1) and (3.19.2) derived by the REP in (3.17) are called **R-SEP1** and **R-SEP2**, respectively.

3.3. Error analysis

In this subsection, we will discuss residuals of QEP (3.1) and REP (3.8) by using linearizations (3.7.1) and (3.19.1), respectively.

We first derive residual bounds of approximate eigenpairs for QEP (3.1) by by using linearizations **Q-SEP1** and **Q-SEP2**, respectively. Let $(\mu_1^{-1},[\mathbf{v}_1^{\top},\mathbf{u}_1^{\top}]^{\top})$ be an approximate eigenpair of (3.7.1) and $[\mathbf{f}_{11}^{\top},\mathbf{f}_{12}^{\top}]^{\top}$ be the associated residual vector. That is,

$$\begin{bmatrix}\mathbf{f}_{11}\\ \mathbf{f}_{12}\end{bmatrix}=\begin{bmatrix}0 & -\widetilde{M}_u\\ \widetilde{K}_u^{-1} & -\widetilde{K}_u^{-1}\widetilde{D}_u\end{bmatrix}\begin{bmatrix}\mathbf{v}_1\\ \mathbf{u}_1\end{bmatrix}-\frac{1}{\mu_1}\begin{bmatrix}\mathbf{v}_1\\ \mathbf{u}_1\end{bmatrix}=\frac{1}{\mu_1}\begin{bmatrix}-\mathbf{v}_1-\mu_1\widetilde{M}_u\mathbf{u}_1\\ \widetilde{K}_u^{-1}(\mu_1\mathbf{v}_1-\mu_1\widetilde{D}_u\mathbf{u}_1-\widetilde{K}_u\mathbf{u}_1)\end{bmatrix}.$$

It follows that

$$\mu_1^2\widetilde{M}_u\mathbf{u}_1+\mu_1\widetilde{D}_u\mathbf{u}_1+\widetilde{K}_u\mathbf{u}_1=\mu_1(-\mathbf{v}_1-\mu_1\mathbf{f}_{11})+\mu_1\mathbf{v}_1-\mu_1\widetilde{K}_u\mathbf{f}_{12}=-\mu_1^2\mathbf{f}_{11}-\mu_1\widetilde{K}_u\mathbf{f}_{12}.$$

Therefore, with $\lambda_1=\mu_1+\sigma$ and from (3.1) we have

$$\frac{\|Q(\lambda_1)\mathbf{u}_1\|}{\|\mathbf{u}_1\|}=\frac{\|\mu_1^2\widetilde{M}_u\mathbf{u}_1+\mu_1\widetilde{D}_u\mathbf{u}_1+\widetilde{K}_u\mathbf{u}_1\|}{\|\mathbf{u}_1\|}\leqslant\frac{|\mu_1|^2\|\mathbf{f}_{11}\|+|\mu_1|\|\widetilde{K}_u\|\|\mathbf{f}_{12}\|}{\|\mathbf{u}_1\|}. \tag{3.20}$$

On the other hand, let $(\mu_2^{-1},[\mathbf{v}_2^{\top},\mathbf{w}_2^{\top}]^{\top})$ be an approximate eigenpair of (3.7.2) and $[\mathbf{f}_{21}^{\top},\mathbf{f}_{22}^{\top}]^{\top}$ be the associated residual vector. That is,

$$\begin{bmatrix}\mathbf{f}_{21}\\ \mathbf{f}_{22}\end{bmatrix}=\begin{bmatrix}0 & -\widetilde{M}_u\widetilde{K}_u^{-1}\\ I & -\widetilde{D}_u\widetilde{K}_u^{-1}\end{bmatrix}\begin{bmatrix}\mathbf{v}_2\\ \mathbf{w}_2\end{bmatrix}-\frac{1}{\mu_2}\begin{bmatrix}\mathbf{v}_2\\ \mathbf{w}_2\end{bmatrix}=\begin{bmatrix}-\widetilde{M}_u\widetilde{K}_u^{-1}\mathbf{w}_2-\frac{1}{\mu_2}\mathbf{v}_2\\ \mathbf{v}_2-\widetilde{D}_u\widetilde{K}_u^{-1}\mathbf{w}_2-\frac{1}{\mu_2}\mathbf{w}_2\end{bmatrix}.$$

It follows that

$$\mu_2^2\widetilde{M}_u\widetilde{K}_u^{-1}\mathbf{w}_2+\mu_2\widetilde{D}_u\widetilde{K}_u^{-1}\mathbf{w}_2+\mathbf{w}_2=\mu_2(-\mathbf{v}_2-\mu_2\mathbf{f}_{21})+\mu_2\mathbf{v}_2-\mu_2\mathbf{f}_{22}=-\mu_2^2\mathbf{f}_{21}-\mu_2\mathbf{f}_{22}.$$

Letting $\mathbf{u}_2=\widetilde{K}_u^{-1}\mathbf{w}_2$, with $\lambda_2=\mu_2+\sigma$ and from (3.1) we have,

$$\frac{\|Q(\lambda_2)\mathbf{u}_2\|}{\|\mathbf{u}_2\|}=\frac{\|\mu_2^2\widetilde{M}_u\mathbf{u}_2+\mu_2\widetilde{D}_u\mathbf{u}_2+\widetilde{K}_u\mathbf{u}_2\|}{\|\mathbf{u}_2\|}\leqslant\frac{|\mu_2|^2\|\mathbf{f}_{21}\|+|\mu_2|\|\mathbf{f}_{22}\|}{\|\mathbf{u}_2\|}. \tag{3.21}$$

Now, we derive residual bounds of approximate eigenpairs for REP (3.8) by using linearizations **R-SEP1** and **R-SEP2**, respectively. Let $(\mu_1^{-1},[\mathbf{s}_1^{\top},\mathbf{p}_1^{\top},\mathbf{q}_1^{\top}]^{\top})$ be an approximate eigenpair of (3.19.1) and $[\mathbf{g}_{11}^{\top},\mathbf{g}_{12}^{\top},\mathbf{g}_{13}^{\top}]^{\top}$ be the associated residual vector. That is,

$$\begin{bmatrix}\mathbf{g}_{11}\\ \mathbf{g}_{12}\\ \mathbf{g}_{13}\end{bmatrix}=\begin{bmatrix}0 & -\widetilde{M}_p & L_p\\ \widetilde{K}_p^{-1} & -\widetilde{K}_p^{-1}\widetilde{D}_p & 0\\ 0 & -\varrho^{-1}R_p^{\top} & \varrho^{-1}\vartheta I_m\end{bmatrix}\begin{bmatrix}\mathbf{s}_1\\ \mathbf{p}_1\\ \mathbf{q}_1\end{bmatrix}-\frac{1}{\mu_1}\begin{bmatrix}\mathbf{s}_1\\ \mathbf{p}_1\\ \mathbf{q}_1\end{bmatrix}.$$

This implies that

$$\mathbf{s}_1=-\mu_1\widetilde{M}_p\mathbf{p}_1+\mu_1L_p\mathbf{q}_1-\mu_1\mathbf{g}_{11}, \tag{3.22}$$

$$\mathbf{g}_{12}=\widetilde{K}_p^{-1}\mathbf{s}_1-\widetilde{K}_p^{-1}\widetilde{D}_p\mathbf{p}_1-\frac{1}{\mu_1}\mathbf{p}_1, \tag{3.23}$$

$$\mathbf{q}_1=\left(\mu_1\varrho^{-1}\vartheta-1\right)^{-1}\mu_1\left(\mathbf{g}_{13}+\varrho^{-1}R_p^{\top}\mathbf{p}_1\right). \tag{3.24}$$

Substituting (3.24) into (3.22), $\mathbf{s}_1$ can be represented by

$$\mathbf{s}_1 = -\mu_1 \widetilde{M}_p \mathbf{p}_1 + \mu_1^2 (\mu_1 \varrho^{-1}\vartheta - 1)^{-1} \left(L_p \mathbf{g}_{13} + \varrho^{-1} L_p R_p^\top \mathbf{p}_1 \right) - \mu_1 \mathbf{g}_{11}. \tag{3.25}$$

Substituting (3.25) into (3.23), from (3.11) and (3.15) we get

$$\begin{aligned} R(\sigma+\mu_1)\mathbf{p}_1 &= \mu_1^2 \widetilde{M}_p \mathbf{p}_1 + \mu_1 \widetilde{D}_p \mathbf{p}_1 + \widetilde{K}_p \mathbf{p}_1 - \mu_1^2 \left[\frac{(\sigma\beta+\alpha)^3}{\alpha^2} + \frac{(\sigma\beta+\alpha)^4}{\alpha^2 \beta \mu_1} \right]^{-1} L_p R_p^\top \mathbf{p}_1 \\ &= -\mu_1^2 \mathbf{g}_{11} - \mu_1 \widetilde{K}_p \mathbf{g}_{12} - \mu_1^2 \left(\frac{\beta}{\sigma\beta+\alpha} + \frac{1}{\mu_1} \right)^{-1} L_p \mathbf{g}_{13} \end{aligned}$$

which implies that

$$\frac{\|R(\sigma+\mu_1)\mathbf{p}_1\|}{\|\mathbf{p}_1\|} \leqslant \frac{1}{\|\mathbf{p}_1\|} \left\{ |\mu_1|^2 \|\mathbf{g}_{11}\| + |\mu_1| \|\widetilde{K}_p\| \, \|\mathbf{g}_{12}\| + \left| \mu_1^2 \left(\frac{\beta}{\sigma\beta+\alpha} + \frac{1}{\mu_1} \right)^{-1} \right| \|L_p\| \, \|\mathbf{g}_{13}\| \right\}. \tag{3.26}$$

On the other hand, let $(\mu_2^{-1}, [\mathbf{s}_2^\top, \mathbf{t}_2^\top, \mathbf{q}_2^\top]^\top)$ be an approximate eigenpair of (3.19.2) and $[\mathbf{g}_{21}^\top, \mathbf{g}_{22}^\top, \mathbf{g}_{23}^\top]^\top$ be the associated residual vector. That is,

$$\begin{bmatrix} \mathbf{g}_{21} \\ \mathbf{g}_{22} \\ \mathbf{g}_{23} \end{bmatrix} = \begin{bmatrix} 0 & -\widetilde{M}_p \widetilde{K}_p^{-1} & \varrho^{-1} L_p \\ I_{n_2} & -\widetilde{D}_p \widetilde{K}_p^{-1} & 0 \\ 0 & -R_p^\top \widetilde{K}_p^{-1} & \varrho^{-1}\vartheta I_m \end{bmatrix} \begin{bmatrix} \mathbf{s}_2 \\ \mathbf{t}_2 \\ \mathbf{q}_2 \end{bmatrix} - \frac{1}{\mu_2} \begin{bmatrix} \mathbf{s}_2 \\ \mathbf{t}_2 \\ \mathbf{q}_2 \end{bmatrix}.$$

This implies that

$$\mathbf{g}_{21} = -\widetilde{M}_p \widetilde{K}_p^{-1} \mathbf{t}_2 + \varrho^{-1} L_p \mathbf{q}_2 - \frac{1}{\mu_2} \mathbf{s}_2, \tag{3.27}$$

$$\mathbf{s}_2 = \widetilde{D}_p \widetilde{K}_p^{-1} \mathbf{t}_2 + \frac{1}{\mu_2} \mathbf{t}_2 + \mathbf{g}_{22}, \tag{3.28}$$

$$\mathbf{q}_2 = \left(\varrho^{-1}\vartheta - \frac{1}{\mu_2} \right)^{-1} \left(R_p^\top \widetilde{K}_p^{-1} \mathbf{t}_2 + \mathbf{g}_{23} \right). \tag{3.29}$$

Substituting (3.28) and (3.29) into (3.27), we have

$$\mu_2^2 \widetilde{M}_p \widetilde{K}_p^{-1} \mathbf{t}_2 + \mu_2 \widetilde{D}_p \widetilde{K}_p^{-1} \mathbf{t}_2 + \mathbf{t}_2 - \mu_2^2 (\vartheta - \varrho\mu_2^{-1})^{-1} L_p R_p^\top \widetilde{K}_p^{-1} \mathbf{t}_2 = -\mu_2^2 \mathbf{g}_{21} - \mu_2 \mathbf{g}_{22} + \mu_2^2 (\vartheta - \varrho\mu_2^{-1})^{-1} L_p \mathbf{g}_{23}.$$

Letting $\mathbf{p}_2 = \widetilde{K}_p^{-1} \mathbf{t}_2$, from (3.11) we get

$$\begin{aligned} R(\sigma+\mu_2)\mathbf{p}_2 &= \mu_2^2 \widetilde{M}_p \mathbf{p}_2 + \mu_2 \widetilde{D}_p \mathbf{p}_2 + \widetilde{K}_p \mathbf{p}_2 - \mu_2^2 \left[\frac{(\sigma\beta+\alpha)^3}{\alpha^2} + \frac{(\sigma\beta+\alpha)^4}{\alpha^2 \beta \mu_2} \right]^{-1} L_p R_p^\top \mathbf{p}_2 \\ &= -\mu_2^2 \mathbf{g}_{21} - \mu_2 \mathbf{g}_{22} + \mu_2^2 \frac{\alpha^2\beta}{(\sigma\beta+\alpha)^4} \left(\frac{\beta}{\sigma\beta+\alpha} + \frac{1}{\mu_2} \right)^{-1} L_p \mathbf{g}_{23}. \end{aligned}$$

Hence,

$$\frac{\|R(\sigma+\mu_2)\mathbf{p}_2\|}{\|\mathbf{p}_2\|} \leqslant \frac{1}{\|\mathbf{p}_2\|} \left\{ |\mu_2|^2 \|\mathbf{g}_{21}\| + |\mu_2| \|\mathbf{g}_{22}\| + \left| \mu_2^2 \frac{\alpha^2\beta}{(\sigma\beta+\alpha)^4} \left(\frac{\beta}{\sigma\beta+\alpha} + \frac{1}{\mu_2} \right)^{-1} \right| \|L_p\| \|\mathbf{g}_{23}\| \right\}. \tag{3.30}$$

Remark 3.1. In order to check the tightness of upper bounds in (3.20) and (3.21), as well as, (3.26) and (3.30) for residuals, respectively, we refer to the coefficient matrices generated in Example 1 of Section 5. For (2.9) we adopt the data as in [4] by setting $\rho = 1$ kg/m^3, $c = 340$ m/s, $\alpha = 5 \times 10^4$ N/m^3, and $\beta = 200$ Ns/m^3. In addition, we choose $\sigma = -25 + 600\pi\imath (\imath \equiv \sqrt{-1})$ as the shift value. Then

(i) from (3.2), the element mass and stiffness matrices are

$$\frac{h^2}{6}\rho \begin{bmatrix} 2 & -1 & 0 \\ -1 & 2 & 0 \\ 0 & 0 & 2 \end{bmatrix}, \quad \rho c^2 \begin{bmatrix} 2 & 2 & 2\sqrt{2} \\ 2 & 2 & 2\sqrt{2} \\ 2\sqrt{2} & 2\sqrt{2} & 4 \end{bmatrix},$$

respectively. Hence, by (3.4) the infinity norm of $\widetilde{K}_u$ can be estimated by $\|\widetilde{K}_u\|_\infty \approx \|K_u\|_\infty = \mathcal{O}(\rho c^2) = \mathcal{O}(10^5)$. From(3.20) and (3.21), we conclude that the upper bound for the residual of the approximate eigenpair $(\mu_1 + \sigma, \mathbf{u}_1)$ of (3.1) by solving **Q-SEP1** is larger than that of the approximate eigenpair $(\mu_2 + \sigma, \mathbf{u}_2)$ of (3.1) by solving **Q-SEP2**.

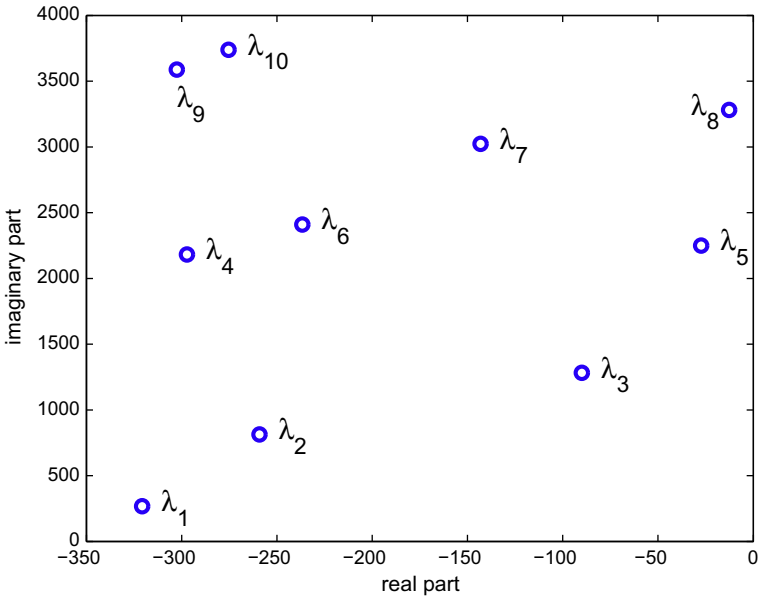

Fig. 2. The distribution of the ten desired eigenvalues $\lambda_1,\ldots,\lambda_{10}$.

(ii) From (3.9), the element mass and stiffness matrices are

$$\frac{h^2}{24}\begin{bmatrix}2&1&1\\1&2&1\\1&1&2\end{bmatrix},\quad \begin{bmatrix}1&-1/2&-1/2\\-1/2&1/2&0\\-1/2&0&1/2\end{bmatrix},$$

respectively. Hence, by (3.14) we have that $\|\widetilde{K}_p\|_\infty \approx \|K_p\|_\infty = \mathcal{O}(1)$. If the eigenvalue λ is one of the desired eigenvalues in Fig. 2, then with $\mu = \lambda - \sigma$ we have

$$4\times 10^7 < \left|\mu^2\left(\frac{\beta}{\sigma\beta+\alpha}+\frac{1}{\mu}\right)^{-1}\right| < 3.1\times 10^{10},$$

$$0.001 < \left|\mu^2\frac{\alpha^2\beta}{(\sigma\beta+\alpha)^4}\left(\frac{\beta}{\sigma\beta+\alpha}+\frac{1}{\mu}\right)^{-1}\right| < 0.8.$$

Clearly, from (3.26) and (3.30) we conclude that the upper bound for the residual of the approximate eigenpair $(\sigma+\mu_1,\mathbf{p}_1)$ of REP (3.8) by solving **R-SEP1** is larger than that of $(\sigma+\mu_2,\mathbf{p}_2)$ of (3.8) by solving **R-SEP2**.

4. Arnoldi method with schur-restarting

The Arnoldi method is the most popular method for solving large sparse SEPs: $\mathcal{L}\mathbf{x}=\lambda\mathbf{x}$. In Arnoldi process, an orthonormal matrix V_{k+1} is generated to satisfy

$$\mathcal{L}V_k = V_kH_k + h_{k+1,k}\mathbf{v}_{k+1}\mathbf{e}_k^\top, \tag{4.1}$$

where $H_k\in\mathbb{R}^{k\times k}$ is upper Hessenberg. If the dimension of the Krylov subspace span $\{V_k\}$ is larger than a certain value, then the process of Arnoldi decomposition will be restarted.

For the restarting process, we can use an implicit restart scheme [17,22]. The package ARPACK[16] includes a very successful implementation of the implicitly restarted Arnoldi algorithm. It has been used by many engineering fields and remains a popular choice for solving eigenvalue problems. However, these implicitly restart type schemes may suffer from numerical instability due to rounding errors. Stewart proposed the Krylov–Schur method [13,23,24] that relaxes the need to preserve the structure of the Arnoldi decomposition and therefore ease the complications of the purging and deflating.

We state the Schur-restarting scheme as follows. Let

$$H_k = [\,U_m \quad U_\ell\,]\begin{bmatrix}T_m & T_f\\0 & T_\ell\end{bmatrix}\begin{bmatrix}U_m^*\\U_\ell^*\end{bmatrix} \tag{4.2}$$

be a Schur decomposition of H_k where T_m and T_ℓ are upper triangular, and the eigenvalues of T_m are of interest. Here and hereafter U^* denotes the conjugate transpose of the matrix U. Substituting (4.2) into (4.1), we see that

$$\mathcal{L}(V_k[U_m \quad U_\ell]) = (V_k[U_m \quad U_\ell])\begin{bmatrix} T_m & T_f \\ 0 & T_\ell \end{bmatrix} + h_{k+1,k}\mathbf{v}_{k+1}(\mathbf{e}_k^\top[U_m \quad U_\ell]),$$

which implies that

$$\mathcal{L}\widetilde{V}_m = \widetilde{V}_m T_m + \tilde{\mathbf{v}}_{m+1}\mathbf{t}_m^*, \tag{4.3}$$

where $\widetilde{V}_m \equiv V_k U_m, \tilde{\mathbf{v}}_{m+1} = \mathbf{v}_{k+1}$ and $\mathbf{t}_m^* \equiv h_{k+1,k}\mathbf{e}_k^\top U_m$. Let Q_1 be a Householder matrix with

$$\mathbf{t}_m^* Q_1 = \tau \mathbf{e}_m^\top.$$

Then (4.3) can be rewritten as

$$\mathcal{L}(\widetilde{V}_m Q_1) = (\widetilde{V}_m Q_1)(Q_1^* T_m Q_1) + \tau\tilde{\mathbf{v}}_{m+1}\mathbf{e}_m^\top. \tag{4.4}$$

The matrix $Q_1^* T_m Q_1$ can be reduced to a new Hessenberg matrix $\widetilde{H}_m$ by using Householder matrices Q_i for $i = 2,\ldots,m-1$ with

$$Q_{m-1}^* \cdots Q_2^*(Q_1^* T_m Q_1)Q_2 \cdots Q_{m-1} = \widetilde{H}_m, \quad \mathbf{e}_j^\top Q_2 \cdots Q_{m-1} = \mathbf{e}_m^\top.$$

Multiplying (4.4) by Q_i, $i = 2,\ldots,m-1$, a new Arnoldi decomposition of order m

$$\mathcal{L}\widetilde{V}_m = \widetilde{V}_m \widetilde{H}_m + \tau\tilde{\mathbf{v}}_{m+1}\mathbf{e}_m^\top$$

is obtained where $\widetilde{V}_m := \widetilde{V}_m Q_1 \cdots Q_{m-1}$ and the Arnoldi process can be applied to generate it to order k in (4.1). One repeats the above process until the desired eigenvalues are convergent. The process is summarized in Algorithm 1.

Algorithm 1. Arnoldi method with Schur-restarting for solving $\mathcal{L}\mathbf{x} = \lambda\mathbf{x}$

Input: $\mathcal{L}$: coefficient matrix, $\mathrm{tol}_{\mathcal{L}}$: tolerance for convergence, $r_{\max}$: maximum number of Schur-restartings.
Output: The desired m eigenpairs.

1: Build an initial Arnoldi decomposition of order m as in (4.1) and set $r = 0$.
2: **restart**
3: Extend Arnoldi decomposition of order m to order $k = m + \ell$ and set $r = r + 1$.
4: Compute all Ritz pairs $(\mu_i^{-1}, \mathbf{z}_i)$ with $H_k\mathbf{z}_i = \mu_i^{-1}\mathbf{z}_i, i = 1,\ldots,k$ and sorting Ritz values so that $\{(\mu_1, z_1),\ldots,(\mu_m, z_m)\}$ are wanted.
5: **for** $i = 1,\ldots,m$
6: Check convergence by $|h_{k+1,k}||\mathbf{e}_k^\top\mathbf{z}_i| < \mathrm{tol}_{\mathcal{L}}$.
7: **end for**
8: **if** (Not all m desired eigenvalues are convergent and $r < r_{\max}$) **then**
9: Compute the Schur decomposition of H_k as in (4.2), where the eigenvalues of T_m are of interest.
10: Set $V_m := V_k U_m$, $\mathbf{v}_{m+1} := \mathbf{v}_{k+1}$ and $\mathbf{t}_m^* := h_{k+1,k}\mathbf{e}_k^\top U_m$.
11: Compute Householder transformation Q_1 such that $\mathbf{t}_m^* Q_1 = \tau\mathbf{e}_m^\top$.
12: Reduce $Q_1^* T_m Q_1$ to a new Hessenberg matrix H_m by using Householder transformations Q_i for $i = 2,\ldots,m-1$.
13: Set $V_m := V_m Q_1 \cdots Q_{m-1}$ and $h_{m+1,m} = \tau$ to get the new Arnoldi decomposition with order m:

$$\mathcal{L}V_m = V_m H_m + h_{m+1,m}\mathbf{v}_{m+1}\mathbf{e}_m^\top. \tag{4.5}$$

14: **end if**
15: **until** (desired m eigenpairs are convergent or $r \geqslant r_{\max}$)

Now, we will apply the Algorithm 1 to solve QEP (3.1) and REP (3.8), respectively, by setting $\mathcal{L}$ to be the coefficient matrices in (3.7.1) and (3.19.1), respectively.

4.1. Stopping criteria for QEPs and REPs

Let $(\mu^{-1}, \mathbf{z})$ be a Ritz pair and satisfy $H_k\mathbf{z} = \mu^{-1}\mathbf{z}$. From (4.1) and **Q-SEP1** in (3.7.1) we have

$$\begin{bmatrix} 0 & -\widetilde{M}_u \\ \widetilde{K}_u^{-1} & -\widetilde{K}_u^{-1}\widetilde{D}_u \end{bmatrix}\begin{bmatrix} V_{k1} \\ V_{k2} \end{bmatrix}\mathbf{z} = \frac{1}{\mu}\begin{bmatrix} V_{k1} \\ V_{k2} \end{bmatrix}\mathbf{z} + h_{k+1,k}\begin{bmatrix} \mathbf{v}_{k+1,1} \\ \mathbf{v}_{k+1,2} \end{bmatrix}\mathbf{e}_k^\top\mathbf{z}, \tag{4.6}$$

where $V_k = \begin{bmatrix} V_{k1} \\ V_{k2} \end{bmatrix}$ and $\mathbf{v}_{k+1} = \begin{bmatrix} \mathbf{v}_{k+1,1} \\ \mathbf{v}_{k+1,2} \end{bmatrix}$ are partitioned with compatible sizes. Using the first equation of (4.6), we can eliminate $V_{k1}\mathbf{z}$ in the second equation and get

$$\frac{\|Q(\lambda)\mathbf{u}_1\|}{\|\mathbf{u}_1\|} = \frac{\|(\mu^2\widetilde{M}_u + \mu\widetilde{D}_u + \widetilde{K}_u)\mathbf{u}_1\|}{\|\mathbf{u}_1\|} = \frac{|\mu||h_{k+1,k}||\mathbf{e}_k^\top\mathbf{z}|\zeta_1}{\|\mathbf{u}_1\|} \equiv q_1(\mu), \tag{4.7}$$

where $\mathbf{u}_1 = V_{k2}\mathbf{z}$, $\lambda = \mu + \sigma$ and $\zeta_1 = \|\mu\mathbf{v}_{k+1,1} + \widetilde{K}_u\mathbf{v}_{k+1,2}\|$. Without ambiguity by using the same notations as above in Algorithm 1, from (4.1) and **Q-SEP2** in (3.7.2) we also have

$$\begin{bmatrix} 0 & -\widetilde{M}_u\widetilde{K}_u^{-1} \\ I & -\widetilde{D}_u\widetilde{K}_u^{-1} \end{bmatrix}\begin{bmatrix} V_{k1} \\ V_{k2} \end{bmatrix}\mathbf{z} = \frac{1}{\mu}\begin{bmatrix} V_{k1} \\ V_{k2} \end{bmatrix}\mathbf{z} + h_{k+1,k}\begin{bmatrix} \mathbf{v}_{k+1,1} \\ \mathbf{v}_{k+1,2} \end{bmatrix}\mathbf{e}_k^\top\mathbf{z}$$

and

$$\frac{\|Q(\lambda)\mathbf{u}_2\|}{\|\mathbf{u}_2\|} = \frac{\|(\mu^2\widetilde{M}_u + \mu\widetilde{D}_u + \widetilde{K}_u)\mathbf{u}_2\|}{\|\mathbf{u}_2\|} = \frac{|\mu||h_{k+1,k}||\mathbf{e}_k^\top\mathbf{z}|\zeta_2}{\|\mathbf{u}_2\|} \equiv q_2(\mu), \tag{4.8}$$

where $\mathbf{u}_2 = \widetilde{K}_u^{-1}V_{k2}\mathbf{z}, \lambda = \mu + \sigma$ and $\zeta_2 = \|\mu\mathbf{v}_{k+1,1} + \mathbf{v}_{k+1,2}\|$. Therefore, $q_1(\mu)$ in(4.7) and $q_2(\mu)$ in (4.8), respectively, can be used as stopping criteria for residuals while Algorithm 1 is applied to solved QEPs(3.1).

Similarly, we can apply Algorithm 1 to solve REPs(3.8). As above, we let $(\mu^{-1}, \mathbf{z})$ be a Ritz pair and satisfy $H_k\mathbf{z} = \mu^{-1}\mathbf{z}$. From (4.1), and **R-SEP1**, **R-SEP2** in (3.19.1) we have

$$\begin{bmatrix} 0 & -\widetilde{M}_p & L_p \\ \widetilde{K}_p^{-1} & -\widetilde{K}_p^{-1}\widetilde{D}_p & 0 \\ 0 & -\varrho^{-1}R_p^\top & \varrho^{-1}\vartheta I_m \end{bmatrix}\begin{bmatrix} V_{k1} \\ V_{k2} \\ V_{k3} \end{bmatrix}\mathbf{z} = \frac{1}{\mu}\begin{bmatrix} V_{k1} \\ V_{k2} \\ V_{k3} \end{bmatrix}\mathbf{z} + h_{k+1,k}\begin{bmatrix} \mathbf{v}_{k+1,1} \\ \mathbf{v}_{k+1,2} \\ \mathbf{v}_{k+1,3} \end{bmatrix}\mathbf{e}_k^\top\mathbf{z} \tag{4.9}$$

and

$$\begin{bmatrix} 0 & -\widetilde{M}_p\widetilde{K}_p^{-1} & \varrho^{-1}L_p \\ I_{n_2} & -\widetilde{D}_p\widetilde{K}_p^{-1} & 0 \\ 0 & -R_p^\top\widetilde{K}_p^{-1} & \varrho^{-1}\vartheta I_m \end{bmatrix}\begin{bmatrix} V_{k1} \\ V_{k2} \\ V_{k3} \end{bmatrix}\mathbf{z} = \frac{1}{\mu}\begin{bmatrix} V_{k1} \\ V_{k2} \\ V_{k3} \end{bmatrix}\mathbf{z} + h_{k+1,k}\begin{bmatrix} \mathbf{v}_{k+1,1} \\ \mathbf{v}_{k+1,2} \\ \mathbf{v}_{k+1,3} \end{bmatrix}\mathbf{e}_k^\top\mathbf{z}, \tag{4.10}$$

where $V_k = [V_{k1}^\top, V_{k2}^\top, V_{k3}^\top]^\top$ and $\mathbf{v}_{k+1} = [\mathbf{v}_{k+1,1}^\top, \mathbf{v}_{k+1,2}^\top, \mathbf{v}_{k+1,3}^\top]^\top$ are partitioned with compatible sizes. Using the first and the third equations of (4.9) and (4.10), we can eliminate $V_1\mathbf{z}$ and $V_3\mathbf{z}$ in the second equation of (4.9) and (4.10), respectively, and get

$$\frac{\|R(\lambda)\mathbf{p}_1\|}{\|\mathbf{p}_1\|} = \frac{\|[\mu^2\widetilde{M}_p + \mu\widetilde{D}_p + \widetilde{K}_p - \mu^2(\vartheta - \varrho\mu^{-1})^{-1}A_p]\mathbf{p}_1\|}{\|\mathbf{p}_1\|} = \frac{|\mu||h_{k+1,k}||\mathbf{e}_k^\top\mathbf{z}|\xi_1}{\|\mathbf{p}_1\|} \equiv r_1(\mu), \tag{4.11}$$

where $\mathbf{p}_1 = V_{k2}\mathbf{z}$, $\lambda = \mu + \sigma$ and $\xi_1 = \|\mu\mathbf{v}_{k+1,1} + \widetilde{K}_p\mathbf{v}_{k+1,2} - \frac{\varrho\mu^2}{\vartheta\mu-\varrho}L_p\mathbf{v}_{k+1,3}\|$, and

$$\frac{\|R(\lambda)\mathbf{p}_2\|}{\|\mathbf{p}_2\|} = \frac{\left\|\left[\mu^2\widetilde{M}_p + \mu\widetilde{D}_p + \widetilde{K}_p - \mu^2(\vartheta - \varrho\mu^{-1})^{-1}A_p\right]\mathbf{p}_2\right\|}{\|\mathbf{p}_2\|} = \frac{|\mu||h_{k+1,k}||\mathbf{e}_k^\top\mathbf{z}|\xi_2}{\|\mathbf{p}_2\|} \equiv r_2(\mu), \tag{4.12}$$

where $\mathbf{p}_2 = \widetilde{K}_p^{-1}V_{k2}\mathbf{z}, \lambda = \mu + \sigma$ and $\xi_2 = \|\mu\mathbf{v}_{k+1,1} + \mathbf{v}_{k+1,2} - \frac{\mu^2}{\vartheta\mu-\varrho}L_p\mathbf{v}_{k+1,3}\|$. Therefore, $r_1(\mu)$ in(4.11) and $r_2(\mu)$ in (4.12) can be used as stopping criteria for residuals while Algorithm 1 is applied to solve REPs (3.8).

Applying Algorithm 1 to solve QEPs (3.1) and REPs (3.8) are summarized in Algorithms 2 and 3, respectively.

Algorithm 2. Arnoldi method with Schur-restarting for solving QEP in (3.1)

Input: Coefficient matrices M_u, D_u and K_u, parameters c, α and β, σ: shift value, tol_Q: tolerance for convergence, $r_{\max}$: maximum number of Schur-restartings.

Output: The desired eigenpairs $(\lambda_i, \mathbf{u}_i)$ for$i = 1, \ldots, m$.

1: Construct matrices $\widetilde{M}_u, \widetilde{D}_u$ and $\widetilde{K}_u$ defined in (3.4) and set $r = 0$.
2: Compute initial Arnoldi decomposition in Line 1 of Algorithm 1 with $\mathcal{L}$ in **Q-SEP1** or **Q-SEP2**.
3: **restart**
4: Do the steps in Lines 3 and 4 of Algorithm 1.
5: **for** $i = 1, \ldots, m$ **do**
6: Compute $\varphi(\mu_i) = (|\sigma + \mu_i^{-1}|^2\|M_u\| + |\alpha + (\sigma + \mu_i^{-1})\beta|\|A_u\| + \|K_u\|)$.
7: **Check convergence** of QEP by $q_\ell(\mu_i)/\varphi(\mu_i) < \mathrm{tol}_Q$ with $q_\ell(\mu_i)$ in (4.7) or (4.8),$\ell = 1,2$.
8: **end for**
9: **if** (Not all m desired eigenvalues are convergent and $r < r_{\max}$) **then**
10: Do the Schur-restarting in Lines 9–13 of Algorithm 1.
11: **end if**
12: **until** (desire m eigenpairs are convergent or $r \geqslant r_{\max}$)
13: Set $\lambda_i = \sigma + \mu_i^{-1}$ and $\mathbf{u}_i = V_{k2}\,\mathbf{z}_i$ for$i = 1, \ldots, m$.
14: **if Q-SEP2** is solved **then**
15: $\mathbf{u}_i \leftarrow \widetilde{K}_u^{-1}\mathbf{u}_i, i = 1, \ldots, m$.
16: **end if**

Algorithm 3. Arnoldi method with Schur-restarting for solving REP in (3.8)

Input: Coefficient matrices M_p, K_p and A_p, parameters c, α and β, σ: shift value, tol_R: tolerance for convergence, $r_{\max}$: maximum number of Schur-restartings.

Output: The desired eigenpairs $(\lambda_i, \mathbf{p}_i)$ for $i = 1,\ldots,m$.

1: Construct matrices $\widetilde{M}_p, \widetilde{D}_p$ and $\widetilde{K}_p$ defined in (3.12), (3.13) and (3.14), respectively, and set $r = 0$.
2: Compute the full-rank decomposition of A_p:$L_p R_p^\top = A_p$.
3: Compute initial Arnoldi decomposition in Line 1 of Algorithm 1 with $\mathcal{L}$ in **R-SEP1** or **R-SEP2**.
4: **restart**
5: Do the steps in Lines 3 and 4 of Algorithm 1.
6: **for** $i = 1,\ldots,m$ **do**
7: Compute $\psi(\mu_i) = |\frac{(\sigma+\mu_i^{-1})^2}{c^2}|\|M_p\| + \|K_p\| + |\frac{(\sigma+\mu_i^{-1})^2}{\alpha+(\sigma+\mu_i^{-1})\beta}|\|A_p\|$.
8: **Check convergence** by $r_\ell(\mu_i)/\psi(\mu_i) <$ tol_R with $r_\ell(\mu_i)$ in (4.11) or(4.12),$\ell = 1,2$.
9: **end for**
10: **if** (Not all m desired eigenvalues are convergent and $r < r_{\max}$) **then**
11: Do the Schur-restarting in Lines 9–13 of Algorithm 1.
12: **end if**
13: **until** (desire m eigenpairs are convergent or $r \geqslant r_{\max}$)
14: Set $\lambda_i = \sigma + \mu_i^{-1}$ and $\mathbf{p}_i = V_{k2}\,\mathbf{z}_i$ for $i = 1,\ldots,m$.
15: **if R-SEP2** is solved **then**
16: $\mathbf{p}_i \leftarrow \widetilde{K}_p^{-1}\mathbf{p}_i, i = 1,\ldots,m$.
17: **end if**

4.2. Computational costs

In this subsection, we compare the computational costs of the jth Arnoldi step of Algorithm 1 for solving **Q-SEP**s (3.7.1) and **R-SEP**s (3.19.1), respectively. This is of general interest, because a comparison of the CPU times is sensible only if the number of outer iterations of Algorithm 2 or Algorithm 3 is the same for each algorithm. From (4.5), the unit vector $\mathbf{v}_{j+1}$ is generated by

$$\mathcal{L}\mathbf{v}_j = \sum_{i=1}^{j} h_{j,i}\mathbf{v}_i + h_{j+1,j}\mathbf{v}_{j+1}$$

where $h_{j,i} = \mathbf{v}_i^* \mathcal{L}\mathbf{v}_j$ for $i = 1,\ldots,j$ and $h_{j+1,j} = \|\mathcal{L}\mathbf{v}_j - \sum_{i=1}^{j} h_{j,i}\mathbf{v}_i\|_2$. For convenience, we let $\mathbf{v}_j = [\mathbf{v}_{j1}^\top, \mathbf{v}_{j2}^\top]^\top$ with $\mathbf{v}_{ji} \in \mathbb{C}^n$, $i = 1,2$. The matrix–vector product $\mathcal{L}\mathbf{v}_j$ in Algorithm 2 for solving QEP (3.1) by **Q-SEP1** (3.7.1) and **Q-SEP2** (3.7.2) can be, respectively, represented by

$$\mathcal{B}_u^{-1}\mathcal{A}_u\mathbf{v}_j = \begin{bmatrix} -\widetilde{M}_u\mathbf{v}_{j2} \\ \widetilde{K}_u^{-1}(\mathbf{v}_{j1} - \widetilde{D}_u\mathbf{v}_{j2}) \end{bmatrix}, \quad \mathcal{A}_u\mathcal{B}_u^{-1}\mathbf{v}_j = \begin{bmatrix} -\widetilde{M}_u\mathbf{g}_u \\ \mathbf{v}_{j1} - \widetilde{D}_u\mathbf{g}_u \end{bmatrix}$$

with $\mathbf{g}_u = \widetilde{K}_u^{-1}\mathbf{v}_{j2}$. This implies that Algorithm 2 for **Q-SEP1** and **Q-SEP2** needs the same computational costs for generating the unit vector $\mathbf{v}_{j+1}$ for each j.

On the other hand, by letting $\mathbf{v}_j = [\mathbf{v}_{j1}^\top, \mathbf{v}_{j2}^\top, \mathbf{v}_{j3}^\top]^\top$ with $\mathbf{v}_{ji} \in \mathbb{C}^n, i = 1,2$ and $\mathbf{v}_{j3} \in \mathbb{C}^m$, the matrix–vector product $\mathcal{L}\mathbf{v}_j$ in Algorithm 3 for solving REPs by **R-SEP1** (3.19.1) and **R-SEP2** (3.19.2) can be, respectively, represented by

$$\mathcal{B}_p^{-1}\mathcal{A}_p\mathbf{v}_j = \begin{bmatrix} L_p\mathbf{v}_{j3} - \widetilde{M}_p\mathbf{v}_{j2} \\ \widetilde{K}_p^{-1}(\mathbf{v}_{j1} - \widetilde{D}_p\mathbf{v}_{j2}) \\ \varrho^{-1}\vartheta\mathbf{v}_{j3} - \varrho^{-1}R_p^\top\mathbf{v}_{j2} \end{bmatrix}, \quad \mathcal{A}_p\mathcal{B}_p^{-1}\mathbf{v}_j = \begin{bmatrix} \varrho^{-1}L_p\mathbf{v}_{j3} - \widetilde{M}_p\mathbf{g}_p \\ \mathbf{v}_{j1} - \widetilde{D}_p\mathbf{g}_p \\ \varrho^{-1}\vartheta\mathbf{v}_{j3} - R_p^\top\mathbf{g}_p \end{bmatrix}$$

with $\mathbf{g}_p = \widetilde{K}_p^{-1}\mathbf{v}_{j2}$. Consequently, the computational cost of $\mathcal{A}_p\mathcal{B}_p^{-1}\mathbf{v}_j$ needs an extra cost for the computation of $\varrho^{-1}(L_p\mathbf{v}_{j3})$ compared to that $\mathcal{B}_p^{-1}\mathcal{A}_p\mathbf{v}_j$. The cost for generating the unit vector $\mathbf{v}_{j+1}$ by **R-SEP1** is slightly cheaper than that by **R-SEP2**. We summarize the computational costs of generating $\mathbf{v}_{j+1}$ for by **Q-SEP2** and **R-SEP2** in Table 1.

Table 1
Computational costs of the jth Arnoldi step of Algorithm 1 for **Q-SEP2** and **R-SEP2**, where $\widetilde{M}_u, \widetilde{D}_u, \widetilde{K}_u \in \mathbb{R}^{n_1\times n_1}$, $\widetilde{M}_p, \widetilde{D}_p, \widetilde{K}_p \in \mathbb{R}^{n_2\times n_2}$ and $L_p, R_p \in \mathbb{R}^{n_2\times m}$ with $m \ll n_2$. The length of the vectors in the inner products for **Q-SEP2** and **R-SEP2** are $2n_1$ and $2n_2 + m$, respectively.

	Q-SEP2 (3.7.2)	**R-SEP2** (3.19.2)
Solving linear system	$\widetilde{K}_u\mathbf{x}_u = \mathbf{b}_u$	$\widetilde{K}_p\mathbf{x}_p = \mathbf{b}_p$
Matrix–vector products	$\widetilde{M}_u\mathbf{b}_u, \widetilde{D}_u\mathbf{b}_u$	$\widetilde{M}_p\mathbf{b}_p, \widetilde{D}_p\mathbf{b}_p, L_p\mathbf{c}_p, R_p^\top\mathbf{c}_p^\top$
Inner products	$j+1$	$j+1$
Saxpy operators	$j+1$	$j+2$
Scale-vector product	1	1

Remark 4.1. In the numerical implementation, the vectors $\mathbf{g}_u = \widetilde{K}_u^{-1}\mathbf{v}_{j2}$ and $\mathbf{g}_p = \widetilde{K}_p^{-1}\mathbf{v}_{j2}$ for $j = 1,\ldots,k$ can be saved in $G_u \equiv [\widetilde{K}_u^{-1}\mathbf{v}_{12}\cdots\widetilde{K}_u^{-1}\mathbf{v}_{k2}]$ and $G_p \equiv [\widetilde{K}_p^{-1}\mathbf{v}_{12}\cdots\widetilde{K}_p^{-1}\mathbf{v}_{k2}]$, respectively, so that the vectors $\mathbf{u}_2$, $\mathbf{p}_2$ in (4.8) and (4.12) can be computed by $\mathbf{u}_2 = G_u\mathbf{z}$ and $\mathbf{p}_2 = G_p\mathbf{z}$ directly. Hence, it requires the same computational costs for computing $\mathbf{u}_1$, $\mathbf{u}_2$ in (4.7) and (4.8), as well as, $\mathbf{p}_1$, $\mathbf{p}_2$ in (4.11) and (4.12), respectively. Consequently, the computational costs of **Q-SEP1** for the convergence test in Algorithm 2 need one extra matrix–vector product $\widetilde{K}_u\mathbf{v}_{k+1,2}$ than those of **Q-SEP2** in computing ζ_1 and ζ_2. Similarly, the computational costs of **R-SEP1** for the convergence test in Algorithm 3 need one extra matrix–vector product $\widetilde{K}_p\mathbf{v}_{k+1,2}$ than those of **R-SEP2** in computing ξ_1 and ξ_2. Therefore, we conclude that Algorithm 2 for **Q-SEP1** and **Q-SEP2**, as well as, Algorithm 3 for **R-SEP1** and **R-SEP2**, respectively, almost have the same computational costs provided that they have the same outer iterations.

5. Numerical results

We conduct numerical experiments to evaluate performance and accuracy of the eigenvalue solvers described in Section 4. To distinguish between various eigenvalue problems, we use notations **Q1**, **Q2**, **R1** and **R2** defined as follows:

- **Q1**: Applying Algorithm 2 to solve the QEP (3.1) with **Q-SEP1** in (3.7.1).
- **Q2**: Applying Algorithm 2 to solve the QEP (3.1) with **Q-SEP2** in (3.7.2).
- **R1**: Applying Algorithm 3 to solve the REP (3.8) with **R-SEP1** in (3.19.1).
- **R2**: Applying Algorithm 3 to solve the REP (3.8) with **R-SEP2** in (3.19.2).

All computations are carried out in MATLAB 2009a on a HP workstation with an Intel Quad-Core Xeon X5570 2.93 GHz and 72 GB main memory, using IEEE double-precision floating-point arithmetic. We apply Algorithms 2 and 3 to solve the following examples arising in fluid–solid systems. The order k of Arnoldi decomposition in Line 3 of Algorithm 1 is set $k = 40$, the maximum number $r_{\max}$ of Schur-restartings is set $r_{\max} = 15$ and the number of desired eigenpairs is $m = 10$. The relative residuals of approximate eigenpairs $(\lambda_i, \mathbf{u}_i)$ and $(\lambda_i, \mathbf{p}_i)$ computed by **Q1** and **Q2**, as well as, **R1** and **R2** are, respectively, defined by

$$\frac{\|Q(\lambda_i)\mathbf{u}_i\|}{\varphi(\lambda_i)\|\mathbf{u}_i\|} \quad \text{and} \quad \frac{\|R(\lambda_i)\mathbf{p}_i\|}{\psi(\lambda_i)\|\mathbf{p}_i\|}$$

where $\varphi(\lambda_i)$ and $\psi(\lambda_i)$ are given in Algorithms 2 and 3, respectively. Tolerances for relative residuals of QEPs and REPs are chosen by $\mathrm{tol}_Q = \mathrm{tol}_R = 5\times10^{-15}$. The linear systems in Algorithms 2 and 3 are solved by LU-factorization with the shift value $\sigma = -25 + 600\pi\imath$. Fronbenius norm for matrices and 2-norm for vectors are used.

Example 1 [4]. We take the geometrical data: the domain $\Omega = [0m,1m]\times[-0.75m,0m]$, $\Gamma_A = [0m,1m]\times\{0m\}$ given in Fig. 1(i) and the following physical data: $\rho = 1$ kg/m^3, $c = 340$ m/s, $\alpha = 5\times10^4$ N/m^3, and $\beta = 200$ Ns/m^3.

Table 2
Dimension information and convergence rates of λ_1.

(M,N)	Matrix size (QEP)	Matrix size (REP)		Conv. rate	
	$(3M-1)\times N$	$(M+1)\times(N+1)$	λ_1	**Q2**	**R2**
(48,36)	5,148	1,813			
(96,72)	20,664	7,081			
(192,144)	82,800	27,985	$rate_{[1,1]}$	1.9979	2.0010
(384,288)	331,488	111,265	$rate_{[1,2]}$	1.9995	2.0003
(768,576)	1,326,528	443,713	$rate_{[1,3]}$	1.9999	2.0001

The rectangular domain Ω is uniformly partitioned into M by$N$ rectangles and each rectangle is further refined into two triangles, see Fig. 1(ii). The dimensions of coefficient matrices in QEP(3.1) and REP(3.8) are $(3M-1)\times N$ and $(M+1)\times(N+1)$, respectively. Fig. 2 plots the analytic solutions of the desired eigenvalues $\lambda_1,\ldots,\lambda_{10}$ of (2.5)–(2.8) (see[4]) with the lowest positive vibration frequencies satisfying $0<\frac{Im(\lambda_i)}{2\pi}<600$ Hz.

Convergence test: We first demonstrate convergence rates of **Q2** and **R2** while computing the desired eigenvalues in Fig. 2. To measure the convergence rate, we run the test over the five successively refined meshes (See the first column of Table 2) and then calculate the rates by

$$rate_{[i,j]}=\log_2\left(\frac{|\lambda_{[i,j]}-\lambda_{[i,j+1]}|}{|\lambda_{[i,j+1]}-\lambda_{[i,j+2]}|}\right),\quad \text{for } i=1,\ldots,10,\ j=1,2,3,$$

where $\lambda_{[i,j]}$ for $j=1,\ldots,5$ denote the approximate eigenvalues computed by **Q2** and **R2** corresponding toλ_i obtained from the meshes described in Table 2. The 5th and the 6th columns of Table 2 illustrate the quadratic convergence of $rate_{[1,j]}$ {$j=1,2,3$ for λ_1 of QEP (3.1) and REP (3.8), respectively. In our numerical experiment, the convergence rate are always close to 2 for all desired eigenvalues, λ_i, $i=1,\ldots,10$, computed by **Q2** and **R2** as well as **Q1** and **R1**.

Normwise scaling of QEP: Balancing norms of coefficient matrices is an important issue [26] before solving a QEP of the form:

$$P(\mu)x\equiv(\mu^2P_2+\mu P_1+P_0)x=0. \tag{5.1}$$

In [10] authors give an elegant way to scale the norms of coefficient matrices of (5.1) as follows. Define

$$\widehat{P}(\nu)x\equiv(\nu^2\widehat{P}_2+\nu\widehat{P}_1+\widehat{P}_0)x=0$$

with $\nu=\mu/\zeta,\widehat{P}_2=\zeta^2\eta P_2,\widehat{P}_1=\zeta\eta P_1$ and $\widehat{P}_0=\eta P_0$, where ζ and η are scaling factors. Taking ζ and η as $\zeta_*=\sqrt{\gamma_0/\gamma_2}$ and $\eta_*=2/(\gamma_0+\gamma_1\zeta_*)$ with $\gamma_2:=\|P_2\|_2,\gamma_1:=\|P_1\|_2,\gamma_0:=\|P_0\|_2$, it is proved in[10] that the problem

$$\min_{\zeta,\eta}\max\left\{|\|\widehat{P}_2\|_2-1|,|\|\widehat{P}_1\|_2-1|,|\|\widehat{P}_0\|_2-1|\right\}$$

achieves the optimum at ζ_* and η_*. In our implementation, the values of γ_i, for $i=0,1,2$ are computed by $\gamma_2=\|\widetilde{M}_u\|_F,\gamma_1=\|\widetilde{D}_u\|_F,\gamma_0=\|\widetilde{K}_u\|_F$ and $\gamma_2=\|\widetilde{M}_p\|_F,\gamma_1=\|\widetilde{D}_p\|_F,\ \gamma_0=\|\widetilde{K}_p\|_F$ for QEP (3.3) and REP (3.17), respectively. We denote "#It" the number of Schur-restartings (outer iterations). In Table 3, we show # Its for computing 10 desired eigenvalues of Example 1 with $(M,N)=(768,576)$ by **Q1**, **Q2**, **R1** and **R2** with/without scaling. The tolerances tol_Q and tol_R for relative residuals are chosen to be 5×10^{-15}. We see that the convergence rate of scaled Q-SEPs or R-SEPs is faster than that of unscaled Q-SEPs or R-SEPs. The performance of **Q2** and **R2** is also better than that of **Q1** and **R1**, respectively. In the case of unscaled REP, the norms of $\widetilde{M}_p,\widetilde{D}_p$ and $\widetilde{K}_p$ in (3.12)–(3.14) are $\mathcal{O}(10^{-10}),\mathcal{O}(10^{-5})$ and $\mathcal{O}(1)$, respectively. Since the norms of coefficient matrices vary too much, **R1** can even fail to converge to 10 eigenpairs after 15 outer iterations.

No spurious eigenmodes: In [4], it has been proved that there are no spurious eigenmodes for the discretization based on Raviart–Thomas finite elements. We compute twenty desired eigenvalues of QEP(3.1) and REP(3.8) by **Q2** and **R2**, respectively, with scaling and various mesh sizes as shown in Table 2 (we computed 20 instead of 10 eigenvalues to be better confirmed). The desired eigenvalues of REP are in one-to-one correspondence to those of QEP which match well with relative error less than 10^{-6}, that is, no spurious eigenmodes ever appear. We numerically conclude that there are no spurious eigenmodes for the discretization in terms of pressure nodal finite elements.

Null space considerations: Theorem 1 shows that the dimension of the null space of QEP (3.1) is equal to the number of interior nodes, i.e., $(M-1)(N-1)$. In order to observe the interference of such a large null space in the convergence of **Q1** and **Q2**, we give six different shift values denoted by the "+" in Fig. 3 to observe variation in the #Its for **Q1** and **Q2**. The integer pair (i,j) under each shift value "+" denotes the#Its for **Q1** and **Q2**, respectively. The results in Fig. 3 shows that the #It needed decreases, as the shift value σ is chosen relatively far away from zero.

Comparison of pressure and displacement formulations: In this paragraph, we shall discuss the advantages of using the nodal pressure finite elements with various mesh sizes described in Table 2. The notations "T_{Q2}" and "T_{R2}" denote the total CPU times for **Q2** and **R2**, respectively. We summarize the results as follows:

- Accuracy of eigenpairs: From Remark 3.1, the upper bound for relative residual of the approximate eigepairs of QEP (3.1) (or REP (3.8)) by using **Q-SEP2** (3.7.2) (or **R-SEP2** (3.19.2)) is much smaller than that by using **Q-SEP1** (3.7.1) (or **R-SEP1** (3.19.1)). On applying **Q1** and **Q2** to solve QEP (3.1) with#It = 2, in Fig. 4, we see that the relative residuals of eigenpairs

Table 3
#Its for $\lambda_1,\ldots,\lambda_{10}$ of Q-SEPs and R-SEPs with/without scaling.

	Q1	Q2	R1	R2
#It (scaled)	3	2	4	3
#It (unscaled)	4	3	15	3

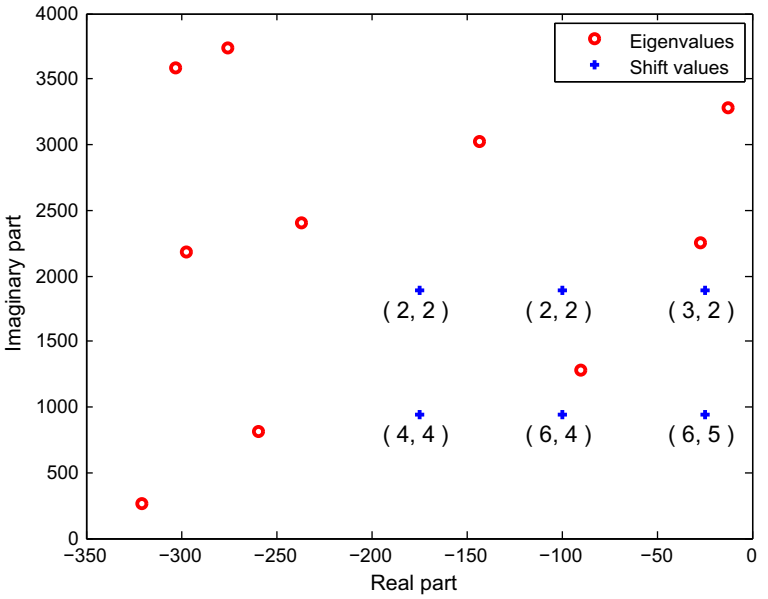

Fig. 3. The #Its of **Q1** and **Q2** with different shift values. "o" denotes desired eigenvalues $\lambda_1,\ldots,\lambda_{10}$. "$(i,j)$" denotes the #Its for **Q1** and **Q2**, respectively.

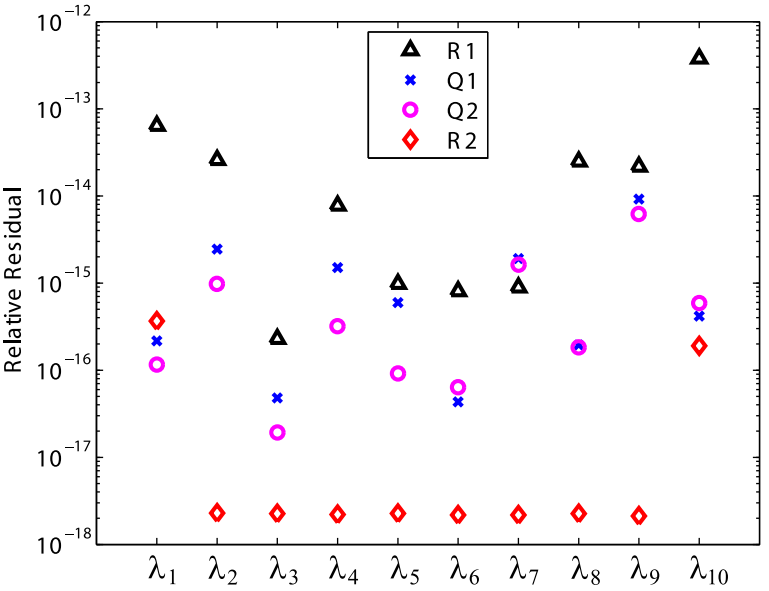

Fig. 4. The relative residuals of computed eigenpairs, obtained by **Q1**, **Q2** for QEP (3.1) and **R1**, **R2** for REP (3.8) with $(M,N) = (768,576)$.

Table 4
Iteration numbers and CPU times for **Q2** and **R2**.

(M,N)	**Q2**		**R2**		$\frac{T_{R2}}{T_{Q2}}$
	#It	T_{Q2}	#It	T_{R2}	
(48,36)	2	1.316	2	0.471	0.36
(96,72)	2	7.717	2	2.387	0.31
(192,144)	2	55.27	2	14.95	0.27
(384,288)	2	567.8	2	134.0	0.24
(768,576)	2	8152	2	1645	0.20

corresponding to λ_4 and λ_5 computed by **Q2** are improved by about 1 significant digit than those by **Q1**. The other eigenpairs almost have the same accuracy. On applying **R1** and **R2** to solve REP (3.8) with#It = 2, in Fig. 4, we see that the relative residuals of eigenpairs computed by **R2** are improved by about 2 to 4 significant digits than those by **R1**.

- Comparison **R2** with **Q2**: From Sub Section 4.2 we see that **Q1** and **Q2**, as well as, **R1** and **R2** have the same computational costs, respectively. From Fig. 4, we favor applying **Q2** and **R2** to solve QEP (3.1) and REP (3.8), respectively. From column 12 of Table 4, we see that the CPU times for solving the REP (3.8) by **R2** is only 1/5 to 1/3 of that for solving the QEP (3.1) by **Q2**. The accuracy of the computed eigenpairs for REP (3.8) is also better than that of QEP (3.1). These results tell us that using **R2** to solve nodal pressure finite elements for the discrete problem (2.12) is better than that using **Q2** to solve Raviart–Thomas displacement finite elements for the discrete problem (2.11).

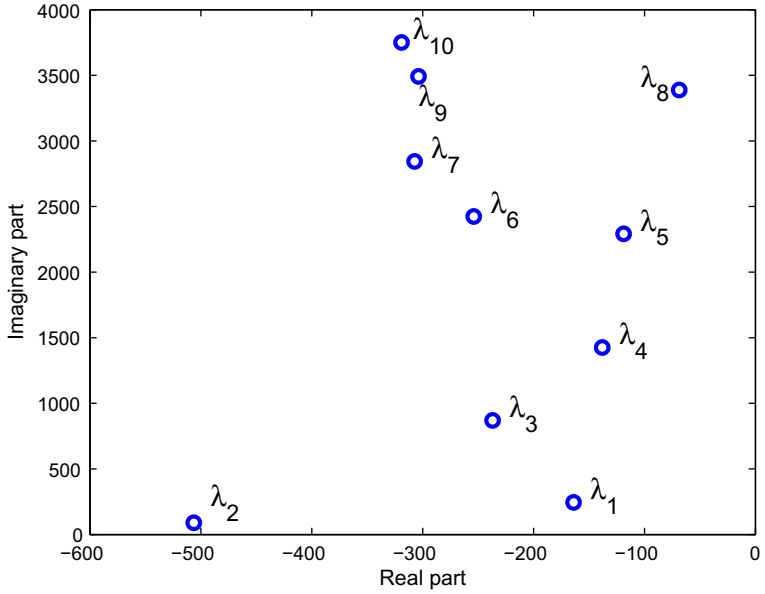

Fig. 5. The distribution of the ten desired eigenvalues $\lambda_1,\ldots,\lambda_{10}$ for Example 2.

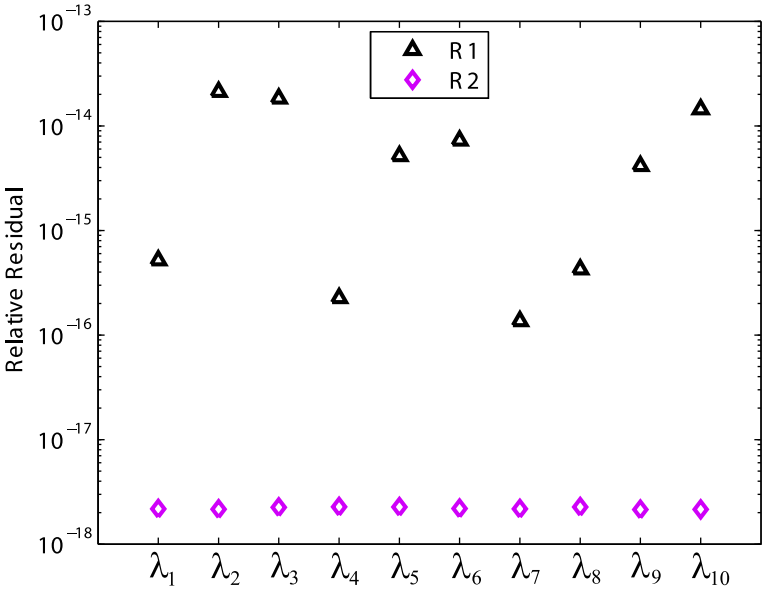

Fig. 6. Relative residuals of computed eigenpairs obtained by **R1** and **R2** for REP in Example 2 with $(M,N) = (768,576)$.

We now want to apply our methods to a more complicated configuration in which the absorbing walls are located on three sides.

Example 2. We use the same geometric data and physical data in Example 1 except that the absorbing wall is extended to one half of the rigid walls in the left and right boundaries, that is $\Gamma = [0,1] \times \{0\} \cup \{0\} \times [-0.375,0] \cup \{1\} \times [-0.375,0]$.

In Example 1, we numerically show that there are no spurious eigenmodes for the discretization in terms of pressure nodal finite elements. Moreover, the computational cost for solving the associated REP (3.8) is obviously less than that of solving QEP (3.1) which is obtained from using Raviart–Thomas displacement finite elements to the discrete problem (2.11). Therefore, in this example we only use nodal finite elements to discretize the model and compare the accuracy of **R1** and **R2** for solving the associated REP. The computed eigenvalues $\lambda_1,\ldots,\lambda_{10}$ with lowest positive vibration frequencies satisfying $0 < \frac{Im(\lambda_i)}{2\pi} < 600$ Hz are shown in Fig. 5. The convergence rates for $\lambda_1,\ldots,\lambda_{10}$ obtained from various the mesh sizes described in Table 2 are also close to 2. The relative residuals computed by **R1** and **R2** are presented in Fig. 6 which shows that the accuracy of the eigenpairs produced by **R2** is better than **R1**.

6. Conclusions

We propose efficient methods for computing damped vibration modes of an acoustic fluid confined in a cavity with absorbing walls capable of dissipating acoustic energy. Two approximations are investigated, one constructed from the edge-based displacement space, which results in QEPs (3.1) and one from the node-based pressure space, which results in REPs (3.8). Our numerical results show that both nodal and edge-based finite elements have second-order convergence rate. We theoretically prove that the nullity of the QEP (3.1) equals the number of the interior grid points. Numerical results show that if the shift value is close to zero, then such a large null space interfere with the convergence of the eigensolver. Furthermore, numerical evidence also shows that there are no spurious eigenmodes for the discretization in terms of pressure nodal finite elements and the CPU times for solving the corresponding REP (3.8) are only 1/5 to 1/3 of the CPU times for solving the QEP (3.1).

For solving the nonlinear eigenvalue problems, a linearization and a trimmed-linearization methods are used to linearize QEP (3.1) and REP (3.8) into four different types of SEPs which can be solved by **Q1** and **Q2**, as well as, **R1** and **R2**. Numerical accuracy shows that **Q2** and **R2** algorithms are better than **Q1** and **R1**, respectively.

Acknowledgments

The authors are grateful to the anonymous referees for their useful comments and suggestions. This work is partially supported by the National Science Council and the National Center for Theoretical Sciences of Taiwan.

References

[1] Z. Bai, Y. Su, A second-order Arnoldi method for the solution of the quadratic eigenvalue problem, SIAM J. Matrix Anal. 26 (3) (2005) 640–659.
[2] K.J. Bathe, C. Nitikitpaiboon, X. Wang, A mixed displacement-based finite element formulation for acoustic fluid–structure interaction, Comput. Struct. 56 (1995) 225–237.
[3] A. Bermúdez, R. Durán, M.A. Muschietti, R. Rodríguez, J. Solomin, Finite element vibration analysis of fluid–solid systems without spurious modes, SIAM J. Numer. Anal. 32 (1995) 1280–1295.
[4] A. Bermúdez, R.G. Durán, R. Rodríguez, J. Solomin, Finite Element anlysis of a quadratic eigenvalue problem arising in disspative acoustic, SIAM J. Numer. Anal. 38 (2000) 267–291.
[5] A. Bermúdez, R. Rodríguez, Finite element computation of the vibration modes of a fluid–solid system, Comput. Methods Appl. Mech. Eng. 119 (1994) 355–370.
[6] A. Bermúdez, R. Rodríguez, Modeling and numerical solution of elastoacoustic vibrations with interface damping, Int. J. Numer. Methods Eng. 46 (1999) 1763–1779.
[7] F. Brezzi, M. Fortin, Mixed and Hybrid Finite Element Methods, Springer-Verlag, New York, 1991.
[8] H.C. Chen, R.L. Taylor, Vibration analysis of fluid–solid systems using a finite element displacement formulation, Int. J. Numer. Methods Eng. 29 (1990) 683–698.
[9] S.H. Chou, S. Tang, ConservativeP1 conforming and nonconforming Galerkin FEMs: effective flux evaluation via a non-mixed method approach, SIAM J. Numer. Anal. 38 (2000) 660–680.
[10] H.Y. Fan, W.W. Lin, P. Van Dooren, Normwise scaling of second order polynomial matrices, SIAM J. Matrix Anal. Appl. 26 (2004) 252–256.
[11] L. Gastaldi, Mixed finite element methods in fluid structure systems, Numer. Math. 74 (1996) 153–176.
[12] M. Hamdi, Y. Ouset, G. Verchery, A displacement method for the analysis of vibrations of coupled fluid–structure systems, Int. J. Numer. Methods Eng. 13 (1978) 139–150.
[13] V. Hernandez, JE Roman, A. Tomas, V. Vidal. Krylov–Schur Methods in SLEPc, Technical report, CSE-2008-13, University of California, Davis, USA, 2008. Available online <http://www.grycap.upv.es/slepc>.
[14] T.-M. Hwang, W.-W. Lin, J.-L. Liu, W. Wang, Jacobi–Davidson methods for cubic eigenvalue problems, Numer. Linear Algebr. Appl. 12 (2005) 605–624.
[15] V. Kehr-Kandille, R. Ohayon, Elastoacoustic damped vibrations. Finite element and modal reduction methods, in: O.C. Zienkiewicz, P. Ladev'eze (Eds.), New Advances in Computational Structural Mechanics, Elsevier, Amsterdam, 1992, pp. 321–334.
[16] R.B. Lehoucq, D.C. Sorensen, C. Yang, ARPACK USERS GUIDE: Solution of Large Scale Eigenvalue Problems With Implicitely Restarted Arnoldi Methods, SIAM, Philadelphia, 1998.
[17] R.B. Morgan, On restarting the Arnoldi method for large non-symmetric eigenvalue problems, Math. Comput. 65 (215) (1996) 1213–1230.

[18] P.A. Raviart, J.M. Thomas, A mixed finite element method for second order elliptic problems, Mathematical Aspects of Finite Element Methods, Lecture Notes in Math, vol. 606, Springer-Verlag, Berlin, Heidelberg, 1977, pp. 292–315.
[19] R. Rodríguez, J. Solomin, The order of convergence of eigenfrequencies in finite element approximations of fluid-structure interaction problems, Math. Comput. 65 (1996) 1463–1475.
[20] A. Ruhe, Algorithms for the nonlinear eigenvalue problem, SIAM J. Numer. Anal. 10 (1973) 674–689.
[21] G.L.G. Sleijpen, A.G.L. Booten, D.R. Fokkema, H.A. van der Vorst, Jacobi-Davidson type methods for generalized eigenproblems and polynomial eigenproblems, BIT 36 (1996) 595–633.
[22] D.C. Sorensen, Implicit application of polynomial filters in ak-step Arnoldi method, SIAM J. Matrix Anal. Appl. 13 (1992) 357–385.
[23] G.W. Stewart, A Krylov–Schur algorithm for large eigenproblems, SIAM J. Matrix Anal. Appl. 23 (2001) 601–614.
[24] G.W. Stewart, Addendum to A Krylov–Schur algorithm for large eigenproblems, SIAM J. Matrix Anal. Appl. 24 (2002) 599–601.
[25] Y. Su, Z. Bai. Solving Rational Eigenvalue Problems via Linearization, Technical report, 2008-13, University of California, Davis, USA, 2008. Available online <http://www.cs.ucdavis.edu/research/tech-reports/2008/CSE-2008-13.pdf>.
[26] F. Tisseur, K. Meerbergen, The quadratic eigenvalue problem, SIAM Rev. 43 (2001) 235–286.
[27] H. Voss, An Arnoldi method for nonlinear eigenvalue problems, BIT 44 (2004) 387–401.
[28] H. Voss, Iterative projection methods for computing relevant energy states of a quantum dot, J. Comput. Phys. 217 (2006) 824–833.
[29] X. Wang, K.J. Bathe, Displacement/pressure based mixed finite element formulations for acoustic fluid-structure interaction problems, Int. J. Numer. Methods Eng. 40 (1997) 2001–2017.